MONTE-CARLO RENORMALISATION GROUP FOR LATTICE QCD

Thesis by

Apoorva Patel

In Partial Fulfillment of the Requirements

for the Degree of

Doctor of Philosophy

California Institute of Technology

Pasadena, California.

1984

(Submitted May 23, 1984)

अज्ञानतिमिरान्धस्य ज्ञानांजनशलाकया ।
चक्षुरुन्मीलितं येन तस्मै श्रीगुरवे नमः ।।

Salutations to that noble teacher who with the collyrium-stick of knowledge has opened the eyes of one, blinded by darkness of ignorance.

ACKNOWLEDGEMENTS

I sincerely thank my advisor Geoffery Fox for his constant encouragement and support and also for giving me the complete freedom to do what I wanted.

Special thanks go to Rajan Gupta in collaboration with whom all the numerical work was done and from whom I learnt many tricks of the trade.

I also thank C. W. Dissly and G. Spix of Cray Research, and my collaborators G. Guralnik, T. Warnock and C. Zemach, for making the numerical calculations for SU(3) possible.

It is a pleasure to thank Richard Feynman for his patience in teaching me many things that shaped my outlook towards the subject of High Energy Physics. I am also grateful to David Politzer, John Preskill, Barry Simon, Anna Hasenfratz and Larry Yaffe for many enlightening discussions during my graduate work.

I am fortunate to have friends like Aneesh Manohar, Olivier Martin, Steve Otto, Mohit Randeria, Balachandran Sathiapalan and Hidenori Sonoda, who generously shared their knowledge of physics with me.

ABSTRACT

The properties of the SU(2) and SU(3) lattice gauge theories are investigated using the Real Space Monte-Carlo Renormalisation Group method. The "$\sqrt{3}$ block transformation" is found to be very efficient in this analysis. The non-perturbative β-function is calculated for the SU(2) lattice gauge theory over a large range of couplings and along both the Wilson axis and the Migdal-Kadanoff improved action line. A possible explanation of the observed non-perturbative features of the β-function is given. The same data sample is used to calculate the improved action needed for better numerical simulations, and the results are compared with those obtained using the Migdal-Kadanoff approximate renormalisation and Symanzik's perturbative improvement approach. A similar but less extensive analysis is done for the SU(3) lattice gauge theory as well.

The results indicate that even for the pure gauge theory, the present day Monte-Carlo calculations are far from establishing an agreement with the expected asymptotic scaling. However, an improved action approach, combined with the β-function determined using the Monte-Carlo Renormalisation Group technique, should make it possible to convincingly demonstrate the scaling behaviour in near future.

Table of Contents

Chapter 1

INTRODUCTION

The basic aim of High Energy Physics is to understand what the fundamental constituents of matter are and how they interact with each other. Among the well-known strong, electro-magnetic, weak and gravitational interactions, the latter three have been rather well understood. But the solution of the strong interaction problem has until now eluded the physicists. The only candidate field theory of strong interactions which is both renormalisable and consistent with the known symmetry properties of the hadrons is Quantum Chromo-Dynamics (QCD). It is unambiguously defined and is capable of describing all the experimental data qualitatively. However, even more than a decade after it was first proposed, no one has been able to extract any numbers out of it for direct experimental comparison.

QCD is a gauge theory describing the interaction between spin $\frac{1}{2}$ quarks and massless vector gluons. The difficulty in understanding this theory stems from the fact that though the interaction is weak at short distances, a property known as asymptotic freedom [1], it grows strong at long distances. The observed spectrum consists not of free quarks and gluons, but only of colour singlet bound states called hadrons. In high energy experiments, at large enough momenta where the coupling is weak enough, one can use standard perturbation theory to calculate the consequences of QCD and these do agree with the experimental results qualitatively. But to make contact with the reality one has to solve the problem of how the quarks and the gluons turn into hadrons as the coupling becomes stronger at lower momentum scales. Just using higher and higher order perturbation theory to account for stronger coupling is not

adequate. The renormalisation group equations show that all dimensionful quantities have the non-analytic dependence on the coupling of the form $exp(-g^{-2})$. Moreover, QCD has a non-trivial topological structure [2] and there are configurations such as instantons which also contribute like $exp(-g^{-2})$ to the path integral [3]. An understanding of these non-perturbative effects is essential in an attempt to understand the complex phenomena of confinement and chiral symmetry breaking.

A formulation of QCD on the lattice provides a framework where all the non-perturbative physics is accessible [4]. In particular, the phenomena of confinement and chiral symmetry breaking can be easily explained in the strong coupling limit. However, the connection to the continuum field theory can be made only in the limit of the lattice spacing going to zero. This occurs in the weak coupling limit and therefore one needs to take a smooth limit from the strong coupling region to the weak coupling region. Though an absence of a phase transition between these two regions can explain the presence of confinement and chiral symmetry breaking in the continuum field theory, an agreement with experimental results can only be obtained by an explicit computation in the weak coupling region. In the past few years, great progress has been made in this direction with the help of high order strong coupling expansions and numerical computations in the intermediate coupling region. But still the results are far from the region where the renormalisation group equations can be used to scale them to their continuum value. The main problem is that there is no unique way of defining a lattice theory corresponding to a given continuum limit. A class of lattice theories, differing from each other by irrelevant lattice operators which vanish as the continuum limit is taken, can give the same continuum theory. Since the numerical calculations are severely limited by the available computer power, one needs to pick out from this class of

theories a particular one which is affected the least by the presence of the irrelevant lattice operators and hence allows a smoother extrapolation to the continuum. This is the object of Real Space Monte-Carlo Renormalisation Group (MCRG). The formulation of lattice QCD is presented in Chapter 2 and the MCRG method is described in detail in Chapter 3.

Even in the absence of any quarks, QCD is a highly non-linear field theory of gluons interacting with each other. Phenomena such as confinement are expected to be present even in this truncated version of the theory and so the study of the pure gauge theory is a first step towards the understanding of the non-perturbative physics. This becomes even more compelling when one faces the fact that the numerical simulations with dynamical quarks are more complicated and time-consuming. Hence the numerical studies here are restricted to the pure gauge theory only. The non-perturbative β-function needed to scale the lattice results to continuum is computed in Chapter 4 for the SU(2) and SU(3) lattice gauge theories. Chapter 5 describes a first attempt towards finding a trajectory in the multi-dimensional coupling constant space, along which it would be smoother to take the continuum limit.

REFERENCES

[1] H. D. Politzer, Phys. Rev. Lett. 30 (1973) 1346.

D. J. Gross and F. Wilczek, Phys. Rev. Lett. 30 (1973) 1343.

[2] G. 'tHooft, Nucl. Phys. B138 (1978) 1.

[3] C. Callan, R. Dashen and D. Gross, Phys. Rev. D17 (1978) 2717.

[4] K. G. Wilson, Phys. Rev. D10 (1974) 2445.

A. M. Polyakov, unpublished, and Phys. Lett. B59 (1975) 82.

Chapter 2

LATTICE GAUGE THEORIES

2.1 : Quantum Field Theory on a Lattice

A common disease of the continuum field theories is the ubiquitous presence of ultraviolet divergences. This singular small distance behaviour can be seen most easily in the perturbative expansion. To make any sense out of these theories, it is necessary to remove these infinities using some kind of regularisation prescription. Many such prescriptions exist in literature and the lattice is just one of them. However, it has an important advantage – that it makes the theory well-defined independent of the perturbation theory, unlike all the other known cut-offs. Such an unambiguous definition is necessary to study the non-perturbative phenomena. On the lattice the internal degrees of freedom of the quantum field theory exist only on a discretised space-time. The Feynman Path Integral then uniquely defines the cut-off theory because the integration is now over a discrete set of variables instead of a space of functions. This makes the lattice formulation very well suited for the study of the non-perturbative phenomena both analytically and numerically. As usual, the continuum theory can be recovered by taking the cut-off to infinity or the lattice spacing to zero.

Let S be the action for the field theory under consideration. Choose the units such that $\hbar = c = 1$. Then, in the Feynman Path Integral approach, there is a phase, e^{iS}, associated with each path which takes the system from one state to another [1]. The total amplitude for a system to evolve from a given initial state to a particular final state is given by the sum of these phases over all possible histories of the system. There is a large amount of cancellation between

the interfering phases, and most of the contribution comes from the paths with stationary phases. This is more easily understood by going to the Euclidean time formulation of the field theory. The complex phase is transformed into an exponentially damping factor and the maximum contribution to the path integral comes from the region where the action is near its minimum. The field theory now becomes just a problem of statistical mechanics, and Monte-Carlo methods can be used to evaluate the path integral. The naive lattice formulation is obtained by replacing the derivatives in the field theory by discrete differences. For example, the action for the $\lambda\varphi^4$ theory becomes,

$$S[\varphi] = \sum_{x,\mu} \frac{a^2}{2}(\varphi(x+\mu)-\varphi(x))^2 + \sum_{x} a^4 \left(\frac{1}{2}m^2\varphi^2(x) + \lambda\varphi^4(x) \right) , \quad (2.1.1)$$

where x labels the lattice sites and μ runs from 1 to 4 in four dimensions. The generating functional for this theory is,

$$Z[J] = \int [d\varphi]\, e^{-S[\varphi] + \sum_{x} J(x)\varphi(x)} . \quad (2.1.2)$$

The lattice regularisation destroys the Lorentz invariance of the theory in a strong manner and consequently the bare Lagrangian is not constrained to be of any particular form by renormalisability arguments. However, this is not expected to cause any serious problem and one hopes to recover the continuum limit smoothly as the lattice spacing $a \to 0$.

The lattice formulation of the gauge theories is a little more tricky. In these theories, local gauge invariance is an intrinsic part of the dynamics and hence one does not want to lose it while formulating the theory on lattice. Explicit gauge invariance requires one to introduce the exponential of the path-ordered line integral of the gauge field $A_\mu(x)$, called the connection, between split point operators,

$$K(1,2) = \exp \left[ig \int_{1}^{2} dx^\mu A_\mu(x) \right] . \quad (2.1.3)$$

As shown by Wilson [2] and Polyakov [3], the exactly gauge invariant lattice theory is conveniently formulated in terms of these connections between adjacent lattice sites, $U_\mu(x) \in SU(N)$,

$$U_\mu(x) \;=\; \exp\left[\, i a g \; A_\mu(x) \,\right], \tag{2.1.4}$$

rather than the gauge fields $A_\mu(x)$. Here $A_\mu(x)$ are the group matrices in the fundamental representation† and the variable $U_\mu(x)$ lives on the link going from the site x to the site $x+\mu$. The reversed link element is defined by,

$$U_{-\mu}(x+\mu) \;=\; U_\mu^\dagger(x)\,. \tag{2.1.5}$$

The gauge invariant action is defined in terms of closed loops of these link matrices. The simplest choice is,

$$\begin{aligned} S[U] \;&=\; \frac{2N}{g^2} \sum_{x,\mu,\nu} \left(1 - \mathrm{Re}\; Tr(U_{plaq})\right), \\ U_{plaq} \;&=\; U_\mu(x)\; U_\nu(x+\mu)\; U_{-\mu}(x+\mu+\nu)\; U_{-\nu}(x+\nu)\,, \end{aligned} \tag{2.1.6}$$

where the traces are normalised to unity. In the limit of $a \to 0$, the exponential in Eq.(2.1.4) can be expanded in powers of a and one can show that,

$$S[U] = \frac{a^4}{4} \sum_x Tr(F_{\mu\nu}(x) F^{\mu\nu}(x)) + \textit{Higher order terms in } a\,, \tag{2.1.7}$$

where the antisymmetric field tensor is defined by,

$$F_{\mu\nu} \;=\; \partial_\mu A_\nu \;-\; \partial_\nu A_\mu \;+\; ig\,\left[\, A_\mu\,,\, A_\nu \,\right]. \tag{2.1.8}$$

The generating functional of the theory becomes,

$$Z \;=\; \int [dU]\, e^{-S[U]}\,, \tag{2.1.9}$$

† In general, the representation of the group matrices depends on the representation of the quarks, but we assume that the quarks are in the fundamental representation.

where $[dU]$ represents the gauge invariant Haar measure.

It is important to note here that Eq.(2.1.6) is not the unique choice of the action. Loops of different shape and sizes can also reproduce Eq.(2.1.7) in the continuum limit. The different choices of action differ in the contribution of the higher order terms in the lattice spacing. Since these higher order terms are irrelevant in the continuum field theory, one can try to keep the effect of these unwanted lattice operators to a minimum by forming a judicious linear combination of different loops. This is the goal of MCRG.

The question of introducing quarks on the lattice is even more subtle. The fermion degrees of freedom, $\psi(x)$, are defined on the lattice sites. Under a local gauge transformation $G(x)$, $U_\mu(x)$ and $\psi(x)$ transform according to,

$$U_\mu(x) \rightarrow G(x)\, U_\mu(x)\, G^\dagger(x+\mu)\,,$$

$$\psi(x) \rightarrow G(x)\,\psi(x)\,. \tag{2.1.9}$$

Hence the gauge invariant quantities are the Wilson strings,

$$\psi(x)\; U_\mu(x).....U_\nu(y-\nu)\,\psi(y)\,. \tag{2.1.10}$$

Now we can construct the gauge invariant fermionic action which will reduce to $\int d^4x\; \overline{\psi}(x)\,(\not{\partial}+m)\,\psi(x)$ in the continuum limit,

$$S_F = \kappa \sum_{x,\mu} [\overline{\psi}(x)(r-\gamma_\mu)U_\mu(x)\psi(x+\mu) + \overline{\psi}(x+\mu)(r+\gamma_\mu)U_\mu^\dagger(x)\psi(x)]$$
$$- \sum_x \overline{\psi}(x)\psi(x)\,. \tag{2.1.11}$$

Preservation of the chiral symmetries of the continuum theory on the lattice would require $r=0$. However, in the continuum limit, this gives rise to 2^d fermion flavours in d dimensions instead of one. In four dimensions, a partial diagonalisation can reduce this number to four [4], but no further reduction is

possible. Also, though each flavour has the correct magnitude of the triangle anomaly, the net anomaly cancels out because of contributions of the opposite sign. A way out is to take $r \neq 0$ [4,5]. Then one indeed obtains only one fermion flavour in the continuum limit, but on the other hand all the chiral symmetries get explicitly broken on the lattice. As pointed out by Nielsen and Ninomiya [6], this is a particular case of a more general problem, that with finite range interactions one cannot describe non-vector chiral symmetries on the lattice without introducing extra unwanted fermion species of the opposite handedness. In this dissertation, however, we will deal only with the pure gauge theory and avoid the fermion problem altogether.

2.2 : Renormalisation and Approach to the Continuum

A regularised theory with a finite cut-off can make sense in the continuum only if the physically measurable quantities do not depend on the cut-off in the limit of the cut-off going to infinity. This is the principle of Renormalisation Group (RG). Such a behaviour is possible only when the bare parameters in the action depend on the cut-off in a certain way. If one knows this dependence of the bare parameters on the cut-off, in terms of the scaling functions or the RG equations, then one might as well deal with the theory having a finite cut-off instead of the continuum theory. This does not result in any loss of information as long as one is interested in the behaviour of the theory below the cut-off. This is precisely the situation in trying to understand the low-lying hadron spectrum of QCD using numerical methods.

Following Wilson [7], consider fluid dynamics as an illustrative example. The motion of the fluid on the macroscopic scale, for example waves with wavelengths of the order of metres, is described by hydrodynamics. On a much

smaller atomic scale, one sees the atomic structure of the fluid, and the physics at this scale must be described by the Schrodinger equation for the electrons making up the atoms. On a still smaller scale, one has to deal with the nuclear physics to understand how the nuclei of the atoms are made. However, in hydrodynamics, there is no reference to what is happening at atomic scales except through some of the parameters in the fluid equations, such as the density and the viscosity of the fluid. The description of the fluid at the scale of metres is completely independent of the description of water at the atomic scale, except for a few effective constants. These constants in the macroscopic theory can be determined by solving the theory at the next smaller scale of importance, namely the atomic scale. The parameters of the atomic scales will in turn depend on what is happening at the nuclear scale. But as long as one is dealing with the macroscopic scale and knows the parameters determined by the physics at the atomic scale, one does not have to worry about what is going on at the nuclear scale. One does not have to solve the nuclear physics problem to determine the macroscopic parameters, as long as the parameters of the atomic scale are known, since the effects of the nuclear physics is already contained in the parameters of the atomic physics.

This analogy holds for many physical systems. Generally they have many different physical scales and for each scale there is a separate set of parameters needed to describe the physics. The parameters of one length scale are determined from the parameters of the next smaller length scale. For field theories, the physical laws describing the different length scales do not change from scale to scale. The same field theory applies to all the scales. However, the parameters appearing in the field theory do change from scale to scale; i.e., they get renormalised. One can deal with the theory with a finite cut-off if these renormalised parameters at that scale are known.

First let us discuss the $\lambda\varphi^4$ theory. Instead of the bare coupling constant λ_0, there will now be a momentum dependent effective coupling $\lambda_{eff}(Q)$ which will have to be used to calculate the vacuum expectation values with external momenta of order Q. To determine $\lambda_{eff}(Q)$, consider the diagrams contributing to the four-point function shown in Fig. 1. The first diagram contributes λ_0 to the four-point function. The second diagram contains the integral,

$$\lambda_0^2 \int d^4k \; \frac{1}{(k^2+m^2)\,[(k+q)^2+m^2]} \; , \tag{2.2.1}$$

where $q = q_1 + q_3$. This integral contains a logarithmic divergence, coming from the region, $|k| \gg m, q$. This divergent part can be written as,

$$\int_Q^\infty \frac{d^4k}{k^4} \; , \tag{2.2.2}$$

with $Q \gg m, q$. Though the various momentum intervals $[Q,2Q]$, $[2Q,4Q]$, ... contribute equal and finite amount, the divergence arises because of the fact that there are infinitely many such intervals. The integral over each one of these momentum intervals represents the contribution of that momentum scale to the divergence. This divergent contribution is independent of the external momenta q_i and hence can be combined with the bare parameter λ_0 to form an effective coupling $\lambda_{eff}(Q)$,

$$\lambda_{eff}(Q) = \lambda_0 + (const.)\,\lambda_0^2 \int_Q^\infty \frac{dk}{k} \; . \tag{2.2.3}$$

Most of the divergent contribution can be absorbed into the definition $\lambda_{eff}(2Q)$,

$$\lambda_{eff}(Q) = \lambda_{eff}(2Q) + (const.)\,\lambda_0^2 \int_Q^{2Q} \frac{dk}{k} \; . \tag{2.2.4}$$

Up to the order of approximation we can neglect $O(\lambda_0^3)$ terms and replace λ_0^2 by $\lambda_{eff}^2(2Q)$ in the above equation. Then the equation defines $\lambda_{eff}(Q)$ in terms of $\lambda_{eff}(2Q)$. This is what we set out to prove, namely, to find the new parameters

of the theory in terms of the ones at the next higher momentum scale. This relation can also be expressed in terms of a differential equation,

$$\frac{d\lambda_{eff}(Q)}{d(lnQ)} = -(const.)\,\lambda^2_{eff}(Q) + O(\lambda^3_{eff})\,. \qquad (2.2.5)$$

In the pure gauge QCD, the only bare parameter is the coupling constant g_0. A perturbative calculation shows that the renormalised coupling constant $g = g(a)$ depends on the lattice spacing according to,

$$\beta(g) \equiv a\frac{dg}{da} = \beta_0 g^3 + \beta_1 g^5 + \ldots\,, \qquad (2.2.6)$$

where the first two coefficients in the expansion are independent of the regularisation scheme [8],

$$\beta_0 = (4\pi)^{-2}\,\frac{11N}{3}\,,\quad \beta_1 = (4\pi)^{-4}\,\frac{34N^2}{3}\,. \qquad (2.2.7)$$

If Λ is some physical scale such as Λ_{QCD} (denoted by Λ_L for the lattice regularisation), this relation can also be expressed as,

$$\Lambda_L a \underset{a\to 0}{\sim} [\beta_0 g^2(a)]^{(-\beta_1/2\beta_0^2)} \exp[-\frac{1}{2\beta_0 g^2(a)}]\,. \qquad (2.2.8)$$

Any physical scale (inverse correlation length) in the lattice theory, m, behaves like a constant times Λ as the continuum limit is taken. Therefore, as one approaches the continuum limit the correlation length diverges in terms of the lattice spacing. In the language of statistical mechanics, this can be interpreted as approaching a critical point, corresponding to a second (or higher) order phase transition. One can therefore apply the various techniques developed to study the critical phenomena in statistical mechanics to this field theory problem.

For QCD, the fixed point lies at $g_{bare}=0$, and the positive sign of β_0 means that the coupling grows stronger at longer length scales. Although the physical

quantities of the theory can be obtained only by going arbitrarily close to the fixed point, one can obtain qualitative and semi-quantitative information even far away from the fixed point. A convenient technique is the strong coupling expansion, which is the subject of discussion of the next section. It corresponds to taking a very coarse lattice and developing a perturbative expansion in g^{-1}. Then one can try to see what happens as the lattice is made less and less coarse. If there is a trajectory in the coupling space which leads smoothly (i.e., no phase transitions) from this strong coupling behaviour to the weak coupling behaviour near the fixed point [9], the symmetry properties of the theory will be the same in both the regions. Such an information is invaluable in understanding the phenomena such as confinement and chiral symmetry breaking. The strong coupling expansions have only a finite radius of convergence and the weak coupling expansions are only asymptotic. So at the present the best method to connect these two extreme regimes is numerical simulations. Another point of interest is that as long as one is satisfied with a certain amount of precision in the actual magnitudes of the physical quantities, one does not have to go arbitrarily close to the fixed point. This is because the fixed points have a certain scaling region around them, where the critical properties of the theory are already very close to their behaviour at the fixed point. In particular, it is generally true that the various ratios $\frac{m}{\Lambda}$ attain their critical values faster than the rate at which the renormalisation group invariant scale Λ approaches the behaviour expressed in Eq.(2.2.8)†. For efficient numerical simulations, it is extremely important to find out how far this scaling region extends from the critical point, and this can be studied systematically using MCRG.

† The perturbative corrections to the Λ-parameter in Eq. (2.2.8) are of the form $(1+O(g^2))$. But the deviations of the dimensionless ratios from their fixed point values can be expressed as a power series in the inverse correlation length and these are of the form $(1+O(a/\xi)) \sim (1+O(exp(-g^{-2})))$.

2.3 : Strong Coupling Expansions

When the coupling constant g is large, the Boltzmann factor in the generating functional can be expanded in a power series in terms of the parameter $\beta \equiv \frac{2N}{g^2}$. For the simple plaquette action,

$$Z = \int [dU] \prod_{plaq} \left(\sum_k \frac{\beta^k}{k!} (Re\ Tr(U_{plaq}))^k \right) . \qquad (2.3.1)$$

This expansion is analogous to the high temperature expansion used in statistical mechanics. The expectation value of the observables of interest can now be computed by integrating this series term by term over the link matrices $U_\mu(x)$. Each term in the series is a product of link variables and hence can be represented on the lattice as a graph. The integral over the group space then gives a non-vanishing contribution only when the group indices are contracted in a manner so as to form a group singlet at each link. The two lowest order non-zero group integrals are :

$$\int [dU]\ U_{ij}\ U^\dagger_{kl} = \frac{1}{N} \delta_{il}\ \delta_{jk} , \qquad (2.3.2)$$

$$\int [dU]\ U_{ij}\ U_{kl} \cdots U_{yz} = \frac{1}{N!} \varepsilon_{ik\ldots y}\ \varepsilon_{jl\ldots z} , \qquad (2.3.3)$$

for a product of N $SU(N)$ matrices with $\varepsilon_{ik\ldots y}$ being the totally anti-symmetric tensor of rank N.

For example, consider the expectation value of a simple plaquette,

$$\begin{aligned} <Tr(U_{plaq})> &= \frac{1}{Z} \int [dU]\ Tr(U_{plaq})\ e^{\beta \sum_{plaq} \mathrm{Re}\ Tr(U_{plaq})} \\ &= \frac{1}{1+O(\beta^2)} \int [dU]\ Tr(U_{plaq})\ (\frac{\beta}{2} Tr(U_{plaq} + U^\dagger_{plaq}) + O(\beta^2)) \\ &= \frac{\beta}{2N^2}(1+\delta_{N2}) + O(\beta^2) . \qquad (2.3.4) \end{aligned}$$

Similarly, for any other observable, the lowest order term comes from the graph in which the observable is minimally but completely "tiled" by simple plaquettes

(see Fig. 2). In particular, the expectation value of a Wilson loop behaves like $(\frac{\beta}{2N^2}(1+\delta_{N2}))^{Area}$ in the lowest order. The higher order terms correspond to the non-minimal surfaces and the higher representations tiling the observable. Since the expectation value of a large Wilson loop of size $R\times T$ represents the free energy of a quark and an anti-quark separated by a distance R,

$$<W(R,T)> \sim exp[-V(R)T] ; \qquad (2.3.5)$$

the area law behaviour proved above corresponds to a linearly confining potential [2].

Higher order terms in the strong coupling expansion can be obtained by more sophisticated methods. They utilise character expansions on the group manifold and cluster expansions of statistical mechanics [10]. An important property of these strong coupling expansions is that they have a finite radius of convergence. This is a consequence of the fact that both the range of the integration variables and the number of graphs at a fixed order in β are bounded [11]. In the strong coupling regime, this convergence property rigorously establishes the following results :

(i) Exponential clustering of correlation functions or non-zero mass gap.

(ii) Area law of the Wilson loop or linear confinement of quarks.

Since the strong coupling region corresponds to a coarse lattice, the correlation length here is smaller than the lattice spacing and the fields are dominantly random. As one moves towards the region of smaller g, the fields at neighbouring sites start becoming more and more correlated and a "roughening transition" occurs. The strong coupling series fails to converge beyond this point [10]. This effect shows up as a strong dependence of the value of the observable on the number of terms retained in the expansion (see Fig. 3). Attempts have been made to extrapolate the series beyond its radius of

convergence, but they have not been very successful [10]. The best known solution at present is to use numerical simulations in this intermediate region to interpolate smoothly between the strong and weak coupling results and it is the subject of discussion of the next section.

2.4 : Present Status of Numerical Simulations

As mentioned earlier, the purpose of these numerical simulations is two-fold.

(a) To establish that one can smoothly go from the strong coupling region into the weak coupling region. Then the properties such as confinement, which exist in the strong coupling region, also hold in the weak coupling region.

(b) To go sufficiently deep into the weak coupling region and calculate within a few percent the physical quantities such as the string tension and the hadron spectrum for direct comparison with the experimental data. This is necessary before one can claim that QCD is the theory of the strong interactions.

Extensive numerical studies of the non-abelian lattice gauge theories have been made only for the $SU(2)$ and $SU(3)$ gauge groups. These Monte-Carlo simulations have been fairly successful in realising the first objective, that for the pure gauge theory there is no phase transition in going from the strong coupling region to the weak coupling region [12]. There is a rapid crossover between these two regions due to the roughening transition mentioned earlier, but it does not destroy confinement, and the static quark-anti-quark potential does show a linear behaviour for large separations [13]. However, these results have been obtained near $g^2 \sim 1.6$ for the $SU(2)$ theory and near $g^2 \sim 1.0$ for the $SU(3)$ theory. This value of the coupling is very large and hence a satisfactory

analysis of the weak coupling behaviour, and a demonstration of scaling still remains to be done.

The main limitation of these numerical simulations comes from the fact that the present day computers are capable of dealing with lattices only up to a certain finite size. One needs to take both the continuum and the infinite volume limit before obtaining any sensible results. If ξ is the correlation length on the lattice, then one needs both $a \ll \xi$ and $\xi \ll L$. The available computer power limits the value of $\frac{L}{a}$ one can use, and this value is about 16 for the present day computers. The gauge theory on a lattice of finite size behaves like the quantum field theory at a finite temperature [14]. QCD is not a confining theory at high temperatures, and so as ξ becomes comparable to L, the lattice theory undergoes a finite temperature deconfining transition [15]. This transition is of second order for the $SU(2)$ theory and of first order for the $SU(3)$ theory [16]. For $\xi \sim L$, the finite size effects spoil the behaviour of any observable which depends on the fact that the theory is confining. Since the correlation length varies exponentially with the coupling, Eq.(2.2.8), the range of couplings explored beyond the crossover region has been very small so far. The value of the string tension and the deconfinement transition temperature have been measured in this limited region, but these values do not scale according to the two-loop perturbative formula, Eq.(2.2.8). Attempts have been made to measure the glueball masses as well [17], but these are affected by systematic errors coming from the fact that it is very difficult to observe the signal from an exponentially decaying correlation function at large distances. Hence, the demonstration of scaling for the glueball masses is much more complicated.

Inclusion of quarks into the dynamics of QCD has even more problems. Because of the difficulties related with chiral symmetries, one has to work either with multiple flavours or with an action where the chiral symmetries are

explicitly broken by terms which vanish in the continuum limit. In the first case one loses all the effects of the anomaly while in the second case the approach to the continuum limit becomes more difficult. Moreover, Monte-Carlo calculations involving dynamical fermions require at least an order of magnitude more computer time. Therefore, most of the work involving fermions has been done in the valence approximation, where all the dynamical quark loops are neglected [18]. This approximation has its own systematic errors, which are expected to be small because of the success of the non-relativistic quark model and large N properties of SU(N) theories in describing the hadrons. But there is no estimate of the magnitude of this error, and hence it is difficult to disentangle the effects coming from the fact that one is working in a region far from the critical point. Also without dynamical quarks it is impossible to reliably study the phenomenon of chiral symmetry breaking. There are other sources of error as well, stemming from the fact that when light quarks are included in the theory, one has more parameters to play with (the bare quark masses), and very light particles such as pions get formed. The light particles are not very well simulated on small lattices and so one has to do an extrapolation from large fermion masses to smaller ones.

Despite all these shortcomings, there seems to be a good qualitative agreement between what is expected and what is observed [19]. The strong coupling expansions can fit the observed flavour non-singlet hadron spectrum reasonably well [5]. The agreement is improved by combining the strong coupling expansions with random walk techniques [20]. The fit to the meson masses turns out to be very good, but the baryons are found to be too heavy. The Monte-Carlo simulations have shown that the baryons become lighter at weaker couplings, but they are still rather heavy in the region of couplings investigated, indicating that the strong coupling features have not completely disappeared. On the

other hand, these preliminary investigations have raised the hope that, by finding a better approach to the continuum limit, some day we may be able to conclude that QCD is the correct theory describing the strong interactions.

REFERENCES

[1] R. P. Feynman and A. R. Hibbs, *Quantum mechanics and path integrals* (McGraw-Hill).

[2] K. G. Wilson, Phys. Rev. D10 (1974) 2445.

[3] A. M. Polyakov, unpublished, and Phys. Lett. B59 (1975) 82.

[4] L. H. Karsten and J. Smit, Nucl. Phys. B183 (1981) 103.

[5] K. Wilson, in *New phenomena in subnuclear physics* (Erice 1975), ed. A. Zichichi, Plenum, New York (1977).

[6] H. B. Nielsen and M. Ninomiya, Nucl. Phys. B185 (1981) 20 ; Nucl. Phys. B193 (1981) 173 ; Phys. Lett. 105B (1981) 219.

[7] K. Wilson, in *Recent Developments in Gauge theories* (Cargese 1979), ed . G. 'tHooft et al, Plenum, New York (1980).

[8] H. D. Politzer, Phys. Rev. Lett. 30 (1973) 1346.

D. J. Gross and F. Wilczek, Phys. Rev. Lett. 30 (1973) 1343.

W. Caswell, Phys. Rev. Lett. 33 (1974) 344.

D. R. Jones, Nucl. Phys. B75 (1974) 531.

[9] T. Tomboulis, Phys. Rev. Lett. 50 (1983) 885.

[10] J. M. Drouffe and J. B. Zuber, Phys. Rep. 102 (1983) 1, and references quoted therein.

[11] K. Osterwalder and E. Seiler, Ann. Phys. (NY) 110 (1978) 440.

[12] M. Creutz, Phys. Rev. D21 (1980) 2308 ; Phys. Rev. Lett. 45 (1980) 313.

[13] J. Stack, Phys. Rev. D27 (1982) 412.

M. Creutz and K. J. M. Moriarty, Phys. Rev. D26 (1982) 2166.

D. Barkai, K. J. M. Moriarty and C. Rebbi, Brookhaven Preprint, BNL-34462 (1984).

S. Otto and J. Stack, Caltech Preprint, CALT-68-1113 (1984).

[14] G. 'tHooft, Nucl. Phys. B153 (1979) 141.

[15] B. Svetitsky and L. Yaffe, Nucl. Phys. B210 [FS6] (1982) 423.

L. McLerran and B. Svetitsky, Phys. Lett. 98B (1981) 195.

[16] J. Kuti, J. Polonyi and K. Szlachanyi, Phys. Lett. 98B (1981) 199.

K. Kajantie, C. Montonen and E. Pietarinen, Z. Phys. C9 (1981) 253.

[17] B. Berg and A. Billoire, Nucl. Phys. B226 (1983) 405.

K. Ishikawa, A. Sato, G. Schierholz and M. Teper, Z. Phys. C21 (1983) 167.

B. Berg, A. Billoire, S. Meyer and C. Panagiotakopoulos, Phys. Lett. 133B (1983) 359.

[18] H. Hamber and G. Parisi, Phys. Rev. Lett. 47 (1981) 1792.

E. Marinari, G. Parisi and C. Rebbi, Phys. Rev. Lett. 47 (1981) 1795.

D. Weingarten, Phys. Lett. 109B (1982) 57.

[19] K. C. Bowler, D. L. Chalmers, A. Kenway, R. D. Kenway, G. S. Pawley and D. J. Wallace, Edinburgh University preprint no. 84/295 (1984).

J. P. Gilchrist, G. Schierholz, H. Schneider and M. Teper, DESY preprint, DESY 84-021 (1984).

[20] N. Kawamoto and K. Shigemoto, Nucl. Phys. B237 (1984) 128.

FIGURE CAPTIONS AND FIGURES

[2.1]The diagrams contributing to λ_{eff} in the $\lambda\varphi^4$ theory.

[2.2]The lowest order contribution in the strong coupling expansion of a Wilson loop.

[2.3]Comparison of the strong coupling results for the string tension [10] with the Monte-Carlo data taken from the second reference in [13], for the SU(3) gauge theory. The arrow indicates the roughening transition. The curves are, from top to bottom, the 0^{th}, 11^{th}, 12^{th} and 10^{th} order strong coupling results. The straight line is the expected asymptotic behaviour in the weak coupling region.

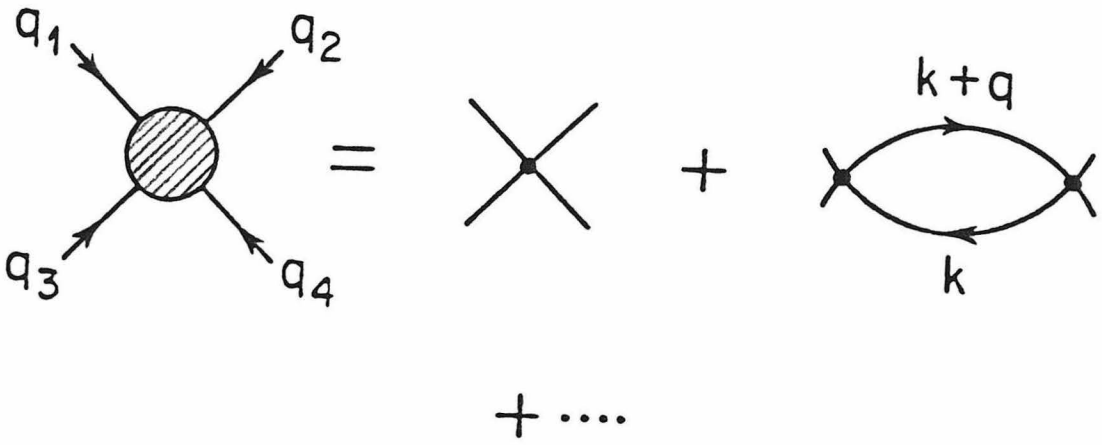

Fig. 2.1

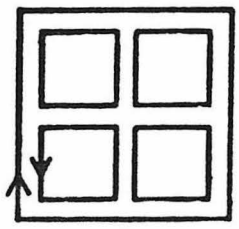

Fig. 2.2

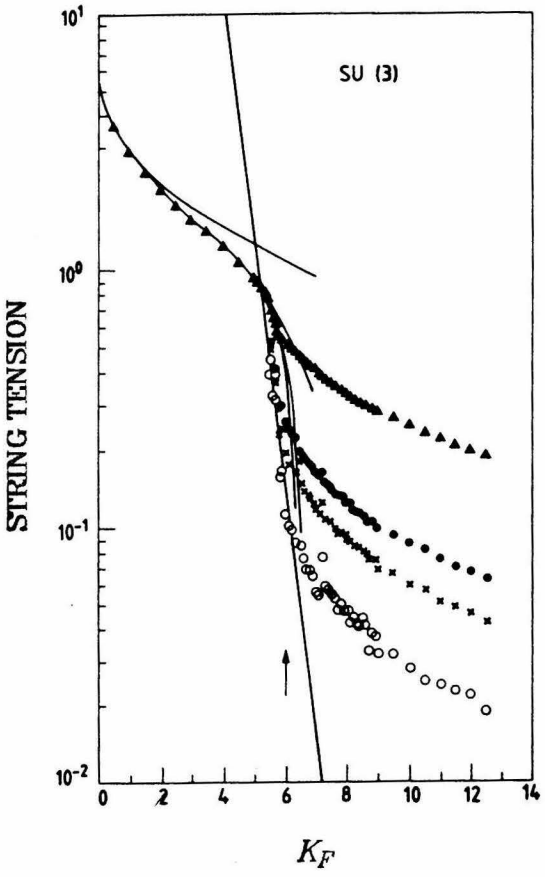

Fig. 2.3

Chapter 3

MONTE-CARLO RENORMALISATION GROUP

3.1 : Renormalisation Group and Fixed Point Theories

As explained in the previous chapter, the renormalisation group (RG) expresses the relation between the parameters of an effective theory, obtained by integrating out the short distance behaviour of a more fundamental theory, and those of the theory at the next smaller length scale. The process of integrating out the short distance behaviour of the theory can be visualised as thinning the degrees of freedom in the partition function by performing a partial functional integration (or summation). Even though the original theory may have only a certain number of interactions, the iterations of the renormalisation process invariably generate an infinite number of interactions among the new variables of the theory. The basic assumption in what follows is that the effective interaction still remains local.

To illustrate these ideas, consider the example of the Ising model. The original Hamiltonian has only nearest neighbour interactions. Now perform the sum over alternate spins in the partition function. This corresponds to a renormalisation group transformation by a scale factor $\sqrt{2}$. The new lattice is hypercubic, but it now has more complicated interactions. As shown in Fig. 3.1, integrating out the spin A creates interactions between the diagonally separated spins B and C, and D and E. A four spin interaction between the spins B, C, D and E is also generated. If this process is iterated a few times, more and more complicated interactions will be generated [1]. The important point is that the strength of these new longer range interactions is much smaller

than that of the original nearest neighbour interaction.

To see the same situation in momentum space, consider the $\lambda\varphi^4$ theory. When the momenta beyond a certain cut-off, $p_i > \Lambda$, are integrated out from the theory, multi-point couplings are generated in the effective theory. For example, Fig. 3.2 shows how two four-point vertices can merge giving rise to a six-point vertex. In field theory, these higher dimensional interactions are called non-renormalisable. They are absent from the original continuum theory and are suppressed by powers of Λ in the effective theory [2].

These simple examples illustrate that, when considering the process of renormalisation, one has to deal with an infinite dimensional coupling constant space. If the original theory is scale invariant, then the renormalisation group transformations will leave it scale invariant. This is the situation for the second order phase transitions in statistical mechanics and the continuum limit of lattice theories. The correlation length, measured in the units of lattice spacing, diverges in these cases. In the infinite dimensional coupling constant space, this limit can be characterised as a subspace, called the critical surface, having $\xi=\infty$. The renormalisation group transformations cannot take a point in this subspace out of it. The most likely situation is that when a number of renormalisation group transformations are performed, the various starting points on the critical surface converge to a particular point on the surface. Such a point is called a fixed point of the theory, since it is invariant under the renormalisation group transformation. In general, the critical surface can have more than one such fixed point, each with its own radius of convergence. However, if one starts slightly off this critical surface, i.e., $\xi\neq\infty$, the renormalisation group transformations monotonically decrease the ratio $\frac{\xi}{a}$, taking the theory farther and farther away from the critical surface. There can be more than one such unstable direction (which in the field theory are characterised by the

renormalisable interactions) orthogonal to the critical surface. Thus if we consider the topology around the fixed point, it looks like a saddle point. The directions which get attracted to the fixed point are called irrelevant, while the directions along which the fixed point is unstable are called relevant. In addition to these, there can exist marginal directions, which are neither attracted nor repelled by the fixed point, but we neglect them for the time being. A typical situation of what happens under successive renormalisation group transformations is shown in Fig. 3.3. The flow of the coupling constants converges towards a subspace characterised by the relevant parameters. When there is only one relevant parameter, this subspace is called the renormalised trajectory (RT), and it is the only direction of instability out of the fixed point.

In the limit of $\xi \to \infty$, the underlying lattice structure of the theory becomes unobservable, and all the physical quantities depend only on the variable ξ. Therefore they either diverge or approach a constant value. In what manner they do so depends on their functional dependence on ξ. This phenomenon is known as scaling in statistical mechanics. For example, for a ferromagnet near its Curie temperature, ξ diverges like a power law, $(T-T_c)^{-\nu}$. Therefore, other quantities such as magnetisation and specific heat also behave like a power of $(T-T_c)$. These powers of $(T-T_c)$, called the critical exponents, are physical observables and can be measured near the critical point of the theory. Different materials with different lattice structures will correspond to different points on the critical surface of the generalised infinite dimensional coupling space. They will be attracted to one or another fixed point on the critical surface. Since the renormalisation group transformation does not change the critical behaviour of the theory, the fixed point will have the same critical behaviour as any other point on the critical surface which is inside its domain of attraction. Different theories which are attracted to the same fixed point will show

the same critical behaviour. This is known as the principle of universality. Thus to find the critical behaviour of a class of theories, all one has to do is to study the behaviour of the generalised theory near its fixed point. Since the critical behaviour of the theory depends only on the rate of divergence away from the critical surface, it depends only on the relevant parameters. Therefore, for practical purposes, working near the fixed point actually helps because the effect of the irrelevant parameters is already negligible there, and one has to worry about only a small dimensional space of relevant parameters. The scaling behaviour and the critical exponents can be found by considering the linearised renormalisation group transformation in the vicinity of the fixed point [3]. This gives the leading behaviour in a certain region around the fixed point. The corrections to this leading behaviour, which include the effect of the marginal operators, can be found by going beyond the linearised transformation [3].

The renormalisation group technique outlined above can be used to study the critical behaviour of any theory with a fixed point. Non-abelian gauge theories possess an ultraviolet fixed point (UVFP) at $g_{bare}=0$ with the correlation length diverging as $\sim exp(\frac{-1}{2\beta_0 g^2})$ [4]. Unlike the statistical mechanics problems, the singularity is not a power law type. It is an essential singularity (or an infinite order phase transition) here. This does not invalidate the use of the technique. The flow away from the fixed point is at a constant rate and the leading corrections to the scaling behaviour are logarithms rather than power law like. This is actually an advantage because it makes the scaling region extend cut to a large g_{bare}.

The continuum non-abelian gauge theories have only one parameter, g_{bare}, and therefore one expects only one direction of divergence, the renormalised trajectory, out of the UVFP. The theory is expected to be confining and so under the renormalisation group transformation one expects to flow from the

UVFP to the trivial infrared fixed point (IRFP). This situation is depicted in Fig. 3.4. The IRFP is completely stable and analogous to the $T=\infty$ trivial fixed point in the statistical mechanics problem. Near the UVFP, the rate of divergence along the RT can be obtained using the linearised transformation and it is given by the perturbative β-function. But away from the UVFP, the presence of phase structures in the infinite dimensional coupling space can distort the RT. Such effects give a non-perturbative contribution to the β-function and also make RT deviate from its linear shape.

Near the UVFP one expects, in principle, very simple scaling properties for physical quantities; i.e., any mass behaves like a constant times Λ_L, where Λ_L is the only renormalisation group invariant mass-scale in the problem. In a lattice calculation performed at a large g_{bare} and on small lattices, irrelevant operators obscure this simple behaviour. The deviations depend both on the distance from the fixed point and on the proximity of phase structure in the infinite dimensional coupling constant space. These local structures can be avoided by using an improved action to approach the continuum limit. The aim is therefore to find an action that has the least effect due to any phase structure and shows scaling at as large a scale as possible.

3.2 : The Real Space Monte-Carlo Renormalisation Group Method

The MCRG method has been developed by Wilson, Kadanoff, Swendsen and Ma [5,6]. It is ideally suited for numerical analysis since the results are not very sensitive to the infrared (small lattice size) cut-off. Thus one can do reliable calculations both near the crossover region and in the weak coupling region. The non-perturbative β-function so found can be used to extrapolate across the region where there are large corrections to the 2-loop perturbative result. This is important because otherwise one is forced to use the

perturbative expressions to extend the results of standard Monte-Carlo calculations done at large g_{bare} to the continuum limit; an assumption that, as the results will show, is unjustified in the range of couplings explored.

To discuss the MCRG method write the lattice action for any given gauge theory as,

$$A[U] = \sum_{\alpha} K_{\alpha} T_{\alpha}[U] , \tag{3.2.1}$$

where the link variables U are elements of the desired gauge group, $\{T_{\alpha}[U]\}$ is the set of all possible gauge invariant traces of Wilson loops and $\{K_{\alpha}\}$ are the corresponding couplings. The change in notation here is for the sake of avoiding complicated expressions. $A[U]$ is just the negative of the U dependent terms in $S[U]$. The partition function for the Euclidean theory is then,

$$Z = \int [dU]\, e^{A[U]} . \tag{3.2.2}$$

In a renormalisation group transformation, the degrees of freedom are thinned by averaging over the short distance fluctuations. This averaging, also called the block transformation, generates a new action on the coarser lattice,

$$A^1[U^1] = R_b(A[U]) = \sum_{\alpha} K_{\alpha}^1 \; T_{\alpha}^1[U^1] . \tag{3.2.3}$$

The link variables U^1 on the blocked lattice are distributed such that,

$$e^{\sum_{\alpha} K_{\alpha}^1 \, T_{\alpha}^1[U^1]} = \int [dU]\, P(U^1,U)\, e^{\sum_{\alpha} K_{\alpha} T_{\alpha}[U]} , \tag{3.2.4}$$

where the block transformation is specified by the probability function $P(U^1,U)$ which defines the relationship between the original degrees of freedom and the block variables. This probability function has to be positive definite, is required to maintain local gauge invariance and satisfy,

$$\int P(U^1,U)\, [dU^1] = 1 . \tag{3.2.5}$$

This condition, Eq. (3.2.5), ensures that the two theories have the same partition function and therefore the same long distance behaviour. Various transformations have been suggested for the gauge theories, and they are described in detail in the next section.

The RG transformation maps a given lattice theory (a point in the coupling constant space) onto another. Under successive RG transformations one generates a trajectory, a flow line of the action. It should be kept in mind that even if one starts out with a single coupling action, the procedure of successive block transformations generates all possible couplings on the lattice. It is in this infinite dimensional coupling constant space $\{K_\alpha\}$, that the non-abelian gauge theories have an ultraviolet fixed point (UVFP) somewhere on the surface $g_{bare}=0$. The exact location of the fixed point and the RT depend on the transformation, while the relation between g_{bare} and the set $\{K_\alpha\}$ is found by examining the coefficient of the $F^{\mu\nu}F_{\mu\nu}$ term for $a\to 0$. Under a scale change all actions that are not on the critical surface flow away from the UVFP towards $g_{bare}\to\infty$ along trajectories that approach the RT. The notion of a β-function therefore exists only along a trajectory. The special status of the RT derives from the fact that it is linear near the UVFP and has smaller corrections due to finite lattice spacing a. Also along it the long distance behaviour of the continuum theory is not modified by irrelevant lattice operators.

An essential ingredient of the RG analysis is that the new couplings $\{K^1_\alpha\}$ are analytic functions of the old $\{K_\alpha\}$. Thus, as long as the range of the interactions stays local and smaller than the lattice size, the results of the MCRG will be governed by the desired UVFP. In renormalisable field theories, the long distance behaviour is controlled by a few (one for QCD) relevant couplings. Since the ideal improved action is given by the basis vector defining the RT, it is hoped that a few local interactions will provide a good approximation to the RT.

In general, points along a co-ordinate line, say $K_{\alpha \neq F} \equiv 0$, are not related by just a change of the scale since other couplings are generated under renormalisation. It is only in the continuum limit $g \to 0$, that the β-function along all trajectories within the universality class will agree with the perturbative result. This is not true at large g. However, Wilson [5] showed a way of calculating the β-function at any arbitrary point that is attracted by the RT. This method is reviewed next.

In Fig. 3.5, the projection of trajectories onto a two coupling constant plane is shown. A and B are two starting points for trajectories that flow to the RT. By adjusting the point B, the n^{th} blocked action, A^n is made to match the $(n-1)^{th}$ blocked action, $B^{(n-1)}$. Thus A^n and $B^{(n-1)}$ have the same correlation length. Then the difference in couplings $\{K_\alpha^A - K_\alpha^B\}$ is the effect of a known scale change, i.e., the scale factor b of the transformation, because the correlation length decreases by a factor b at each blocking. This is precisely the β-function. The equality of the actions A^n and $B^{(n-1)}$ is in practice assumed when a few (~ 10) expectation values match. This assumption can be a posteriori justified if there is only one relevant coupling. In that case all expectation values are correlated, and the matching of a few will guarantee that the rest do too. We have carried out this test by diagonalising the linearised transformation matrix $T_{\alpha\beta}$ and looking at the eigenvalues, and the results do justify the assumption. Lastly, to avoid the effects of the infrared cut-off introduced by a finite lattice, the comparison of the expectation values along the two trajectories is made for the lattices having the same physical size and boundary conditions.

The cook-book recipe for calculating the β-function of the theory can be summarised as follows :

1) The starting couplings $\{K_\alpha^A\}$ and the lattice size (mb^{4n}) are selected.

2) The system is first thermalised. Then the expectation values of the original and blocked Wilson loops are calculated for the n lattices.

3) The starting couplings $\{K_\alpha^B\}$ for the $(mb^{4(n-1)})$ lattice are selected.

4) The corresponding expectation values for the $n-1$ lattices are calculated after thermalisation. These are compared to those obtained in step 2 for the same lattice size.

5) Steps 3 and 4 are repeated until a matching of expectation values at a few different scales implies that the long distance behaviour of the two actions $\{K_\alpha^A\}$ and $\{K_\alpha^B\}$ are related by a scale change of b.

6) The β-function is found by repeating steps 2 to 5 for a number of values of $\{K_\alpha^A\}$. Thus for the non-abelian gauge theories, the quantity calculated using MCRG is,

$$\Delta\beta \;=\; -\frac{\partial(2Ng^{-2})}{\partial(ln\,a)}\cdot lnb \;, \tag{3.2.6}$$

i.e., the discrete approximation to the β-function at g, evaluated for a scale change of b.

A necessary condition for the matching is that the two trajectories A and B track the RT. Even away from the fixed point, the RT is not expected to lose its attractive nature, though as one goes farther from the UVFP, it is likely that the radius of attraction of the RT decreases. Therefore, once the trajectories have come close to the RT, they will flow together with it. To ensure that one remains within the domain of attraction, the starting couplings should be near the UVFP where the RT is attractive and the range of the interactions introduced in the MCRG process should stay smaller than the lattice size. Even then, for an arbitrary starting point, it is only after a certain number of scale changes by a factor of b that the irrelevant couplings obtain their fixed point values. It is

therefore customary to give maximum weight to matching on the smallest lattice (thickest loops). On the other hand, in a Monte-Carlo calculation the block variables are more correlated on coarser lattices. Thus one has to seek a compromise between the statistics and the convergence in the action.

It is desirable to pick the line of starting actions $\{K^A\}$ as close as possible to the RT. There are several ways to find an approximation to the RT, as will be discussed in Chapter 5. One is to use perturbation theory near $g \sim 0$. This programme has been implemented by Wilson [5] and by Symanzik [7]. The other is to use the Migdal-Kadanoff recursion relations [8].

Linearised Transformation

Near the fixed point one can consider the linearised transformation, $T_{\alpha\beta}$, whose eigenvalues give the critical exponents. Universality in fixed point theories states that these exponents (physically measurable quantities) are independent of the transformation. The location of the fixed point and the topology of the critical surface near it, however, depends on the details of the transformation. For asymptotically free theories, the divergence away from the fixed point is at a constant rate and hence the leading eigenvalue of $T_{\alpha\beta}$ is expected to be 1.

In the MCRG method, even though all renormalised couplings of range smaller than the lattice size are automatically included, one does not keep track of them. The matrix $T_{\alpha\beta}$ is instead calculated from fluctuations in the observables, Ω, as,

$$T^n_{\alpha\beta} \equiv \frac{\partial K^n_\alpha}{\partial K^{(n-1)}_\beta} = \frac{\partial K^n_\alpha}{\partial \Omega^n_\sigma} \frac{\partial \Omega^n_\sigma}{\partial K^{(n-1)}_\beta} , \qquad (3.2.7)$$

where the lattice has been blocked n times . Each of the two terms on the right is a connected correlation function, i.e.,

$$\frac{\partial \Omega_\sigma^n}{\partial K_\beta^{(n-1)}} = \langle \Omega_\sigma^n \, \Omega_\beta^{(n-1)} \rangle - \langle \Omega_\sigma^n \rangle \langle \Omega_\beta^{(n-1)} \rangle \ . \qquad (3.2.8)$$

In a practical calculation the number of operators evaluated are few and the correlation functions, Eq. (3.2.8), on blocked lattices require very high statistics.

3.3 : Block Transformations

The fixed point, the renormalised trajectory and the calculational efficiency depend on the renormalisation group transformation. A good transformation will be the one for which the starting line of actions is close to the RT and the RT is fairly attractive in all physically relevant directions. For example, in the simple decimation transformation for the Ising model discussed earlier, the new block variables are the same as the old ones, only the interaction between them is different. Such a crude approximation leaves the correlation functions for the spins σ unchanged, and therefore the scaling index $\frac{\beta}{\nu}$ associated with the spin variables is forced to have the value 0. If the relevant fixed point of the theory has a different value for this scaling index, the flows generated by the decimation transformation will not be attracted by the RT and the transformation will be useless. Such an obvious flaw can be easily seen for a simple transformation like decimation, but for more complicated non-linear transformations it is generally the results that a posteriori justify that the transformation works correctly. In our case, the transformation used in the numerical simulations of the 4-dim non-abelian gauge theories was the "$\sqrt{3}$ block transformation" proposed by Cordery, Gupta and Novotny [9]. But before we discuss it in detail, let us briefly discuss the other two transformations that have been suggested by Wilson [5] and Swendsen [10].

Wilson's Block Transformation

This is a block transformation with $b=2$; i.e., the block site represents a total of $2^4=16$ sites on the original lattice. For the SU(2) theory, the block link variable is defined as the normalised mean of the eight link variables on the original lattice which connect the block y with the block $y+\mu$ (see Fig. 3.6) [5]. The link variables on the original lattice which form the block link do not have identical end points. Hence, the block link variables do not have a simple behaviour under gauge transformations. This is fixed by performing a partial gauge fixing within each block. We need one gauge degree of freedom to be left over for the block site as a whole; therefore the gauge fixing can be done only at 15 of the sites inside each block. Thus there are $64-15=49$ degrees of freedom per block. Only 32 of them are used in the construction of the block links. The remaining degrees of freedom inside each block are taken care of by a block version of Landau gauge fixing; i.e., the sum $\sum_{x,\mu} Tr\, U_\mu(x)$ over all the 32 links that are completely within the block, is maximised with respect to all gauge transformations within the block. More details can be found in the original paper [5].

Swendsen's Block Transformation

This is also a $b=2$ blocking scheme. Here the block link variable is constructed out of nine path ordered products of the link variables on the original lattice [10]. These nine paths connect the nearest neighbour block sites and a 2-dim projection is shown in Fig. 3.7. Since all the nine paths have the same end points, no gauge fixing is needed in this scheme. The central path is topologically different from the rest, and hence has to be considered with a different weight in the construction of the block link variable. Also out of the available 49 degrees of freedom, only 36 are used (9 paths per direction) in this

renormalisation group transformation.

The $\sqrt{3}$ Block Transformation

Before describing the geometry of the transformation, let us first list the advantages of this transformation for a 4-dim hypercubic lattice :

i) The scale factor acts as the independent variable in the discrete derivative defining the β-function, so a small value $b=\sqrt{3}$ is desirable.

ii) The construction of the block variables utilises the maximum number of the degrees of freedom on the starting lattice, while preserving the hypercubic symmetry of the lattice.

iii) There is no gauge fixing required in the construction of the block variables.

iv) Matter fields (complex scalars) defined at the sites can also be simultaneously renormalised, while maintaining exact local gauge invariance of the theory.

Now let us consider the construction of the "block link" variables between the block sites in this transformation. On a 4-dim hypercubic lattice, there are four 3-dimensional positively oriented cubes that originate from a given site. Since the body diagonals of these cubes form an orthogonal set, we use them to define the block lattice. They can be expressed in terms of the original basis vectors $\{e_i\}$ as,

$$\begin{aligned} e_1^1 &= e_3+e_2+e_1 = (0,1,1,1)\,, \\ e_2^1 &= e_4+e_2-e_1 = (1,0,1,-1)\,, \\ e_3^1 &= e_4-e_3+e_1 = (1,-1,0,1)\,, \\ e_4^1 &= e_4+e_3-e_2 = (1,1,-1,0)\,. \end{aligned} \tag{3.3.1}$$

The renormalised lattice so obtained is hypercubical but rotated with respect to the original lattice. The next application of the RG transformation can be selected to undo this rotation by defining the second basis set to be,

$$\begin{aligned} e_1^2 &= e_2^1+e_3^1+e_4^1 = 3e_1 = (3,0,0,0)\,, \\ e_2^2 &= e_1^1-e_3^1+e_4^1 = 3e_2 = (0,3,0,0)\,, \\ e_3^2 &= e_1^1+e_2^1-e_4^1 = 3e_3 = (0,0,3,0)\,, \\ e_4^2 &= e_1^1-e_2^1+e_3^1 = 3e_4 = (0,0,0,3)\,. \end{aligned} \tag{3.3.2}$$

With this construction, all the block sites are a subset of the original lattice. A block site on the renormalised lattice is an average of $b^4=9$ sites on the original lattice. This unit of 9 sites on the original lattice can be thought of as the original sites plus its 8 nearest neighbours. There exists the freedom of which of the 9 sites to call the block site. We have exploited this by summing over all constructions of the blocked lattices, since it improves the statistics significantly. In order to impose periodic boundary conditions, one is constrained to start with a lattice with dimensions that are an integer times a power of the scale factor b. Then a simple way of implementing the periodic boundary conditions on the rotated lattice is to store it as a sub-lattice of the unrotated lattice, which is larger by a factor of b. From Eq.(3.3.1), it can be seen that on a lattice that is an odd power of the scale factor b, the boundary conditions are skewed. This does not affect the calculation of the β-function since there the lattices of the same size (therefore same boundary conditions) are compared. However, more care has to be taken when constructing the 1-step linearised matrix $T_{\alpha\beta}$ to calculate critical exponents since then the boundary conditions are different on the two lattices. A way to measure such an effect is to compare the 2-step linearised matrix (which gives a blocked lattice with the same boundary

conditions as the original one) with the product of two 1-step linearised matrices. This will also indicate the contribution of other finite size effects, for example the ones coming from the creation of interactions of longer range than the lattice size.

The original lattice has 9 lattice sites associated with each block site on the renormalised lattice (the renormalised lattice site and its 8 nearest neighbours). In order that each link be used in the construction of the block link, we need to associate the 36 positively directed links originating from the 9 sites with the 4 positively directed links out of the block site. Eight out of the 36 links can be set equal to the identity by making a gauge transformation at the 8 nearest neighbour sites. The remaining 28 when distributed among the 4 block links correspond to 7 possible links for each block link. These 7 links are shown as heavy lines in Fig. 3.6. The light-lined links in Fig. 3.6 have been gauge fixed to unity. In practice the gauge fixing is taken care of by constructing each of the 7 links as the path ordered product of the 3 links joining the sites on the renormalised lattice. For example, the link U_1 after gauge fixing is the same as the path ordered product $U_a \cdot U_b \cdot U_c$ prior to gauge fixing. One of these paths (labeled U_7) does not connect nearest neighbour sites on the renormalised lattice L^1, but goes along the co-ordinate axis between nearest neighbour sites on the twice renormalised lattice L^2 (e.g. A and D). The remaining 6 topologically identical paths (links labeled U_1, ... U_6 in Fig. 3.6) are the ones that connect the nearest neighbour sites on the renormalised lattice (A and B), and are used to construct the block link. The seventh path can be used in the next reduction but with a different weight than the thick paths. We have chosen to ignore the seventh path altogether and thus we utilise 6 out of every 7 degrees of freedom on the original lattice. The gauge freedom left at the block sites allows this procedure to be repeated for successive applications of the RG transformation.

Having enumerated the paths and shown that their calculation is simple, we now describe the construction of the block link from these paths. A necessary requirement on the transformation is that the local gauge symmetry be preserved. Under a gauge transformation, a link variable, U_{ij}, from site i to site j becomes

$$U_{ij} \rightarrow G_i U_{ij} G_j^{\dagger} \tag{3.3.3}$$

where G_i is the gauge transformation at the site i. Since the 6 paths have the same initial and final points, their mean,

$$\Sigma = \frac{1}{6} \sum_{i=1}^{6} U_i \ , \tag{3.3.4}$$

has the same gauge transformation properties as the individual paths. In the weak coupling limit, averaging the gauge fields is the same as taking Σ to be the block variable. But for larger g_{bare}, Σ is not an element of the group and therefore has to be projected back onto the group manifold. This assumes that no dynamics is lost by throwing away the normalisation†.

For abelian groups and in the special case of SU(2), just the change in normalisation brings back Σ to the group manifold, i.e., $U^1 = normalised(\Sigma)$. This construction can still be used for a discrete subgroup, such as the icosahedral subgroup for SU(2). All that has to be done is to convert the icosahedral elements into the SU(2) matrix representation after update but before blocking. In fact, we found that if this was not done then any transformation that preserves gauge invariance is like a decimation transformation and the theory undergoes rapid disorder. This is discussed in detail later with the data in section 4.3.

† Actually, scaling all the link variables by the same factor is tantamount to a redefinition of the renormalised coupling constants. Therefore, some information about the normalisation does get absorbed in the definition of the renormalised couplings.

For SU(N), N>2, just discarding the normalisation does not bring Σ back to the group manifold. The projection then is defined as the matrix U^1 which maximises $\mathrm{Re}\,Tr\,(\Sigma^\dagger\, U^1)$ [11]. Under a gauge transformation, $\Sigma \rightarrow G\Sigma G^\dagger$ implies that $U^1 \rightarrow GU^1G^\dagger$, and the local gauge invariance is preserved. By polar decomposition,

$$\Sigma \;=\; U\cdot V\cdot De^{i\varphi}\cdot V^\dagger \qquad (3.3.5)$$

where D is a positive definite diagonal matrix and U, V are special unitary matrices. In the weak coupling region, the phase φ is almost zero and U^1 is approximately the same as U. In general, however, the trace maximisation problem has to be solved. This calculation for the gauge group SU(3) is presented in the Appendix. In numerical simulations for SU(3), we tried using both U^1 and U as the possible block link variables, and found that the difference in block loop expectation values at K_F=6.0 was ~1-2% and decreased as K_F was increased. This subtlety is not important in the calculation of the β-function since the same approximation is used for both the lattices.

Inclusion of Matter fields

Let us consider a theory of gauge fields coupled to matter fields $\varphi(x)$ defined at the lattice sites. After the partial gauge fixing at the 8 nearest neighbours of the block site, there is no colour gauge field between the nine sites that form a block. These nine site variables can now be averaged to produce a block variable unambiguously. Thus the block variable $\varphi^1(x)$ is,

$$\varphi^1(x) \;=\; \frac{1}{9}[\varphi(x) + \sum_{\mu}\,(U_\mu(x)\varphi(x+\mu) + U_\mu(x-\mu)^\dagger\varphi(x-\mu))]\,. \qquad (3.3.6)$$

In the real theory of quarks and gluons, the fermions can be represented by complex scalar fields (pseudo-fermions) which have long range interactions.

This interaction range has an exponential damping coming from the quark mass. In the limit of large quark masses, the combined transformation should converge to the fixed point corresponding to the pure gauge theory, since in this limit the quarks decouple from the theory. The interesting case is when the masses are small and especially the chiral limit. The results for the pure gauge theory will bear any relation to this case only if we can make sure that no other fixed point arises as a function of the mass and interchanges stability† with the fixed point of the pure gauge theory. Also one has to make sure that no long range interactions arise in the vanishing mass case, because such a result will violate the fundamental assumption of locality of interactions on which the whole renormalisation group analysis is based. Thus the possibility of renormalising the gauge field together with light matter fields needs to be checked. This is important because the final goal is to find an action that is improved with respect to both the gauge and the matter fields; i.e., we desire the RT for the full theory.

† This situation is known to occur at $d=4$ in case of the ε-expansion [3].

APPENDIX

PROJECTION OF A 3×3 COMPLEX MATRIX ONTO THE SU(3) MANIFOLD

Let Σ be any 3×3 complex matrix. The matrix $\Sigma^{\dagger}\Sigma$ is then Hermitian and positive definite. It can be diagonalised by a unitary transformation,

$$\Sigma^{\dagger}\Sigma \;=\; V\cdot D^{2}\cdot V^{\dagger}\,, \tag{A.1}$$

where V is an SU(3) matrix and D is a positive definite diagonal matrix. Polar decomposition then yields,

$$\Sigma \;=\; P\cdot H \;=\; U\cdot V\cdot D e^{i\varphi}\cdot V^{\dagger}\,, \tag{A.2}$$

where P is a unitary, H is a Hermitian and U is a special unitary matrix. $e^{i\varphi}$ is just a complex phase factor with $\varphi\in[-\frac{\pi}{3},\frac{\pi}{3}]$. Both A and H have 9 degrees of freedom each and together they completely describe the 18 degrees of freedom of Σ. Given any Σ, the diagonalisation in Eq.(A.1) determines V and D. Then inverting Eq.(A.2),

$$U\cdot e^{i\varphi} \;=\; \Sigma\cdot V\cdot D^{-1}\cdot V^{\dagger}\,, \tag{A.3}$$

one can find U and φ.

Now consider the problem of maximising $\mathrm{Re}\,Tr\,(\Sigma^{\dagger}U^{1})$. Let the special unitary matrix Q be defined as,

$$Q \;=\; U^{\dagger}\cdot V^{\dagger}\cdot U^{1}\cdot V\,. \tag{A.4}$$

Then,

$$U^{1} \;=\; U\cdot V\cdot Q\cdot V^{\dagger}\,, \tag{A.5}$$

and,

$$\mathrm{Re}\,Tr(\Sigma^{\dagger}U^{1}) \;=\; \mathrm{Re}\,Tr(De^{-i\varphi}Q)\;. \tag{A.6}$$

Now consider the representation of the 3×3 matrices as three complex column vectors,

$$Q = (\,\vec{X}\;\vec{Y}\;\vec{Z}\,)\;,\;\; De^{i\varphi} = (\,\vec{A}\;\vec{B}\;\vec{C}\,)\;. \tag{A.7}$$

Since Q is an SU(3) matrix, $\vec{X}$, $\vec{Y}$ and $\vec{Z}$ are three orthogonal unit vectors related by $Z = (\vec{X}\times\vec{Y})^{*}$. The diagonal nature of D implies that $\vec{A}$, $\vec{B}$ and $\vec{C}$ are also orthogonal vectors. Therefore,

$$\begin{aligned}\mathrm{Re}\,Tr(De^{-i\varphi}Q) \;&=\; \mathrm{Re}(\vec{A}^{*}\cdot\vec{X} + \vec{B}^{*}\cdot\vec{Y} + \vec{C}^{*}\cdot\vec{Z})\\ &=\; \mathrm{Re}(\vec{A}^{*}\cdot\vec{X} + (\vec{B}^{*} + \vec{C}\times\vec{X})\cdot\vec{Y})\;.\end{aligned} \tag{A.8}$$

For any $\vec{X}$, the quantity on the right-hand side is maximised when,

$$\vec{Y} = \frac{1}{f}(\vec{B} + (\vec{C}\times\vec{X})^{*})\;,\; f \;=\; |\vec{B} + (\vec{C}\times\vec{X})^{*}|\;. \tag{A.9}$$

Choosing this expression for $\vec{Y}$,

$$\mathrm{Re}\,Tr(De^{-i\varphi}Q) \;=\; \mathrm{Re}(\vec{A}^{*}\cdot\vec{X}+f)\;. \tag{A.10}$$

The first term on the right-hand side of the above equation is maximised when $\vec{A}\,||\,\vec{X}$, while the second one is maximised when $\vec{B}\,||\,(\vec{C}\times\vec{X})^{*}$. Both of these conditions are simultaneously satisfied when Q is a complex diagonal matrix. Since $\vec{Y}$ and $\vec{Z}$ are determined once $\vec{X}$ is, to complete the solution we have to find the phase characterising $\vec{X}$. Let this phase be $e^{i\vartheta}$ and d_1, d_2, d_3 be the three eigenvalues of D. Then,

$$\mathrm{Re}\,Tr(De^{-i\varphi}Q) = \mathrm{Re}(d_1e^{i(\vartheta-\varphi)} + f)\;,\;\; f \;=\; |d_2e^{i\varphi} + d_3e^{-i(\vartheta+\varphi)}|\;. \tag{A.11}$$

To maximise this quantity, differentiate with respect to ϑ and obtain,

$$d_1 sin(\vartheta-\varphi)+\frac{1}{f}d_2 d_3 sin(\vartheta+2\varphi) \;=\; 0\,. \qquad \text{(A.12)}$$

This transcendental equation can be solved numerically to complete the solution for U^1. In practice, $\varphi\sim 0$ implies $\vartheta\sim 0$ and the iterative Newton-Ralphson method can be successfully used to find ϑ within $\sim 2-3$ iterations. A good starting guess for ϑ is,

$$\vartheta_0 \;=\; \frac{d_1 d_2 + d_1 d_3 - 2 d_2 d_3}{d_1 d_2 + d_2 d_3 + d_3 d_1}\,\varphi\,. \qquad \text{(A.13)}$$

REFERENCES

[1] K. G. Wilson, Rev. Mod. Phys. 47 (1975) 773.

[2] J. Polchinski, Nucl. Phys. B231 (1984) 269.

[3] K. G. Wilson and J. Kogut, Phys. Rep. 12C (1974) 75.

[4] H. D. Politzer, Phys. Rev. Lett. 30 (1973) 1346.

D. J. Gross and F. Wilczek, Phys. Rev. Lett. 30 (1973) 1343.

[5] K. Wilson, in *Recent Developments in Gauge Theories* (Cargese 1979), ed. G. 't Hooft et al., Plenum Press, New York (1980).

[6] S. K. Ma, Phy. Rev. Lett. 37 (1976) 461.

L. P. Kadanoff, Rev. Mod. Phy. 49 (1977) 267.

R. H. Swendsen, Phys. Rev. Lett. 42 (1979) 859.

R. H. Swendsen, in *Phase Transitions (Cargese 1980)*, ed. M. Levy et al, Plenum Publishing, New York, (1982), and references therein.

S. H. Shenker and J. Tobochnik, Phys. Rev. B22 (1980) 4462.

[7] K. Symanzik, in *Mathematical Problems in Theoretical Physics*, ed. R. Schrader et al., Springer, Lecture Notes in Physics 153 (1982).

[8] A. A. Migdal, Zh. Eksp. Teor. Fiz. 69 (1975) 810.

L. P. Kadanoff, Ann. Phys. 100 (1976) 359.

[9] R. Cordery, R. Gupta and M. Novotny, Phys. Lett. B128 (1983)

[10] R. H. Swendsen, Phys. Rev. Lett. 47 (1981) 1775.

[11] R. Gupta, A. Patel, G. Guralnik, T. Warnock and C. Zemach, Northeastern preprint, NUB-2635 (1984).

FIGURE CAPTIONS AND FIGURES

[3.1]A decimation transformation for the Ising model. Crosses represent the spins on the original lattice which get integrated in the process of RG transformation.

[3.2]The integration of high momentum contribution in the $\lambda\varphi^4$ theory gives rise to six-point vertices in the effective theory.

[3.3]The flow of coupling constants near the fixed point.

[3.4]The renormalised trajectory for non-abelian gauge theories.

[3.5]The evolution of actions under the renormalisation transformation. The two actions $\{K^A\}$ and $\{K^B\}$ have the same long distance behaviour and their lattice correlation length is related by the scale transformation b.

[3.6]The block transformation proposed by Wilson. Dots and crosses represent the sites on the original and blocked lattice, respectively. The lines represent the links on the original lattice used in the construction of the block link.

[3.7]The block transformation suggested by Swendsen. The open circles represent the sites on the blocked lattice. A, B and C are three of the paths used in the construction of the block link.

[3.8]The geometry of the $\sqrt{3}$ transformation.

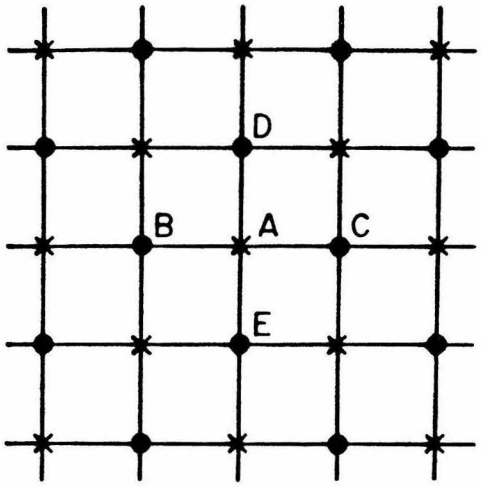

Fig. 3.1

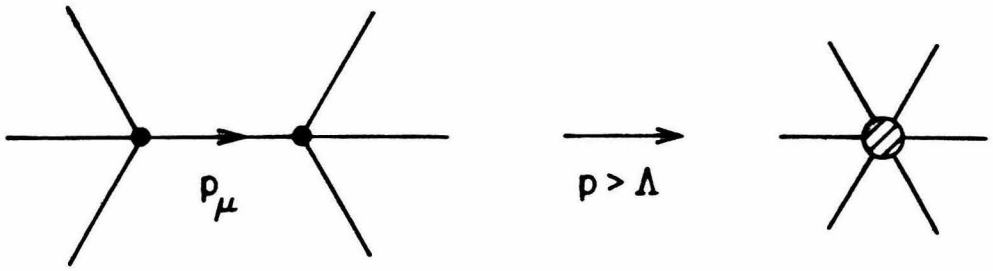

Fig. 3.2

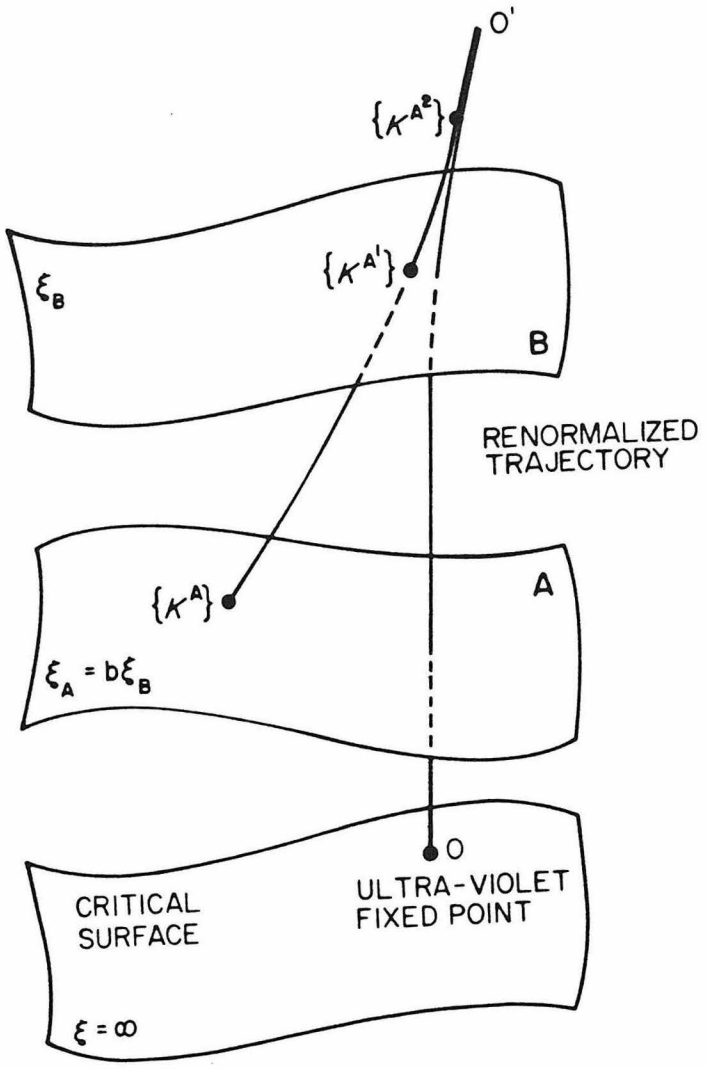
O'
$\{K^{A^2}\}$
$\{K^{A'}\}$
ξ_B
B
RENORMALIZED
TRAJECTORY
$\{K^A\}$
A
$\xi_A = b\xi_B$
O
ULTRA-VIOLET
FIXED POINT
CRITICAL
SURFACE
$\xi = \infty$

Fig. 3.3

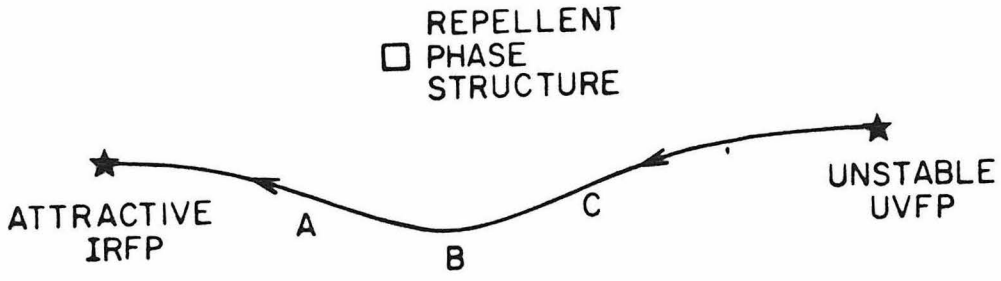
REPELLENT
PHASE
STRUCTURE
ATTRACTIVE
IRFP
A
B
C
UNSTABLE
UVFP

Fig. 3.4

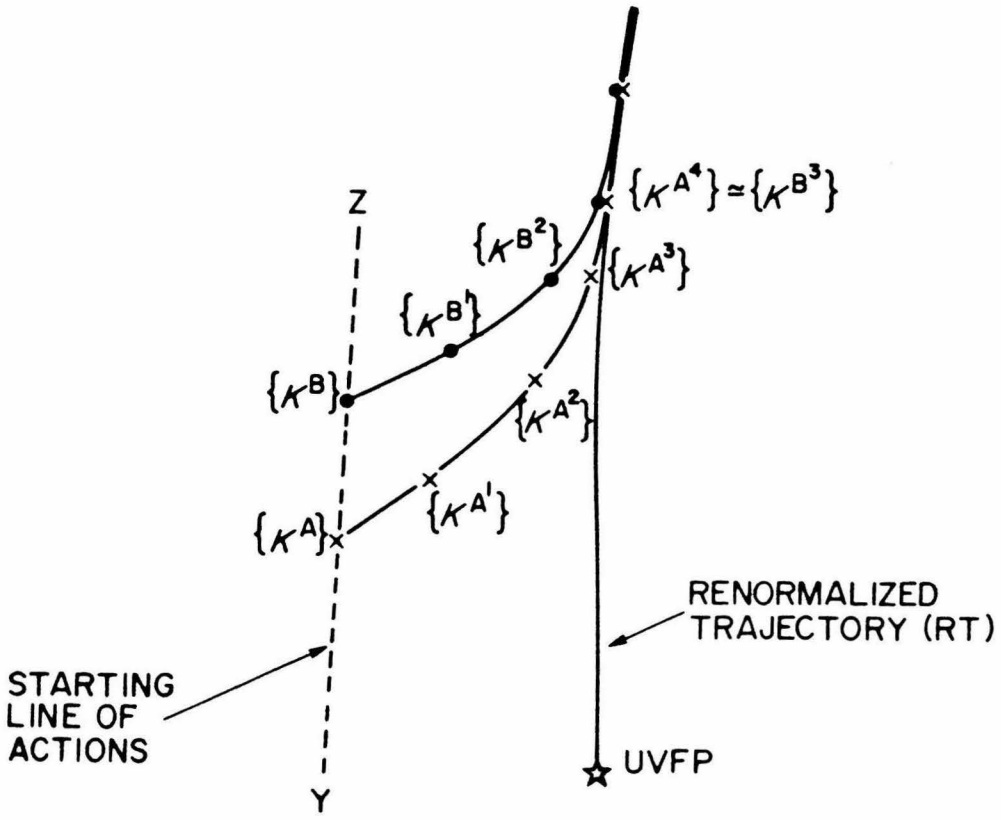
Z
$\{\kappa^{A^4}\} \simeq \{\kappa^{B^3}\}$
$\{\kappa^{B^2}\}$
$\{\kappa^{A^3}\}$
$\{\kappa^{B'}\}$
$\{\kappa^{B}\}$
$\{\kappa^{A^2}\}$
$\{\kappa^{A'}\}$
$\{\kappa^{A}\}$
RENORMALIZED
TRAJECTORY (RT)
STARTING
LINE OF
ACTIONS
UVFP
Y

Fig. 3.5

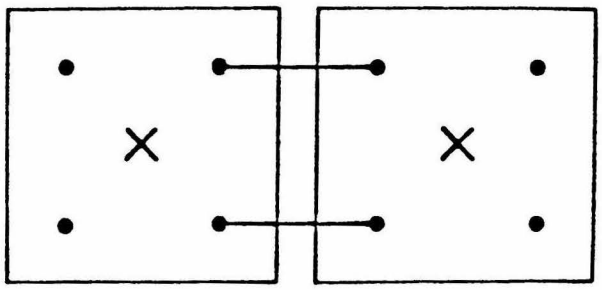

Fig. 3.6

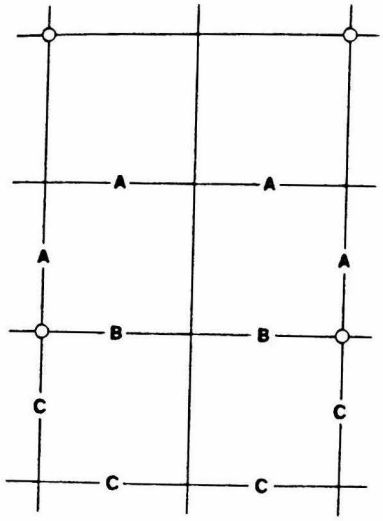

Fig. 3.7

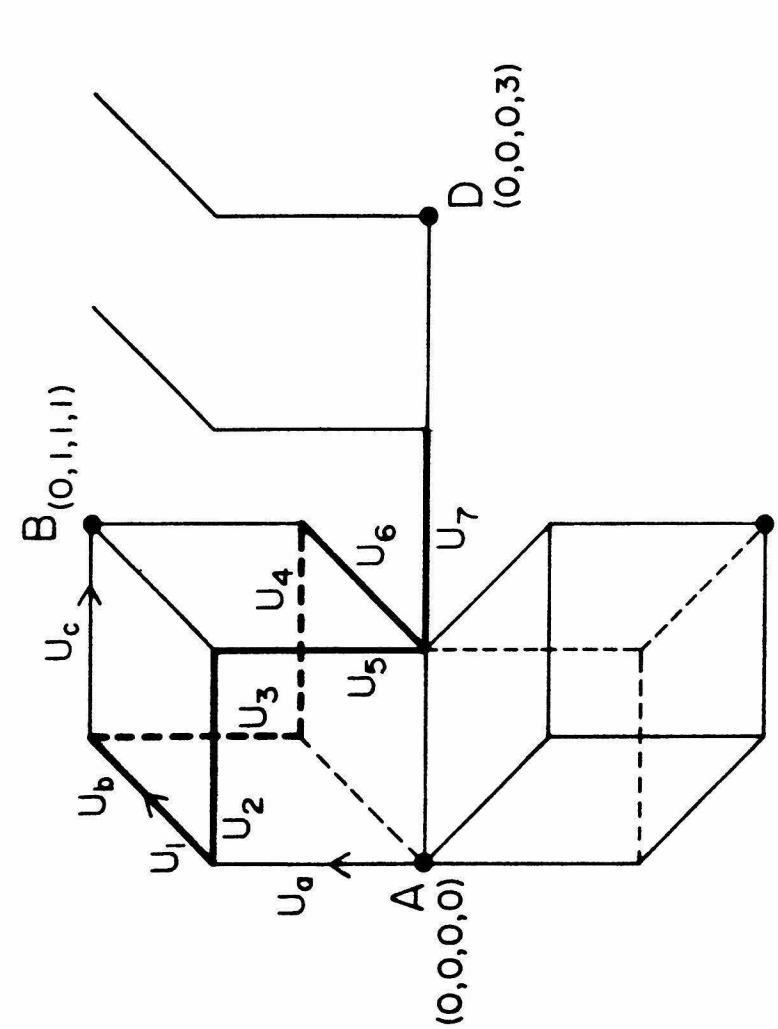

4-DIMENSIONAL HYPERCUBIC LATTICE

Fig. 3.8

Chapter 4

THE β-FUNCTION

4.1 : Scaling Limit and Finite Size Effects

The β-function measures the rate of change of the coupling g with respect to the change in the ultraviolet cut-off a. The 2-loop perturbative result has already been mentioned in Eqs.(2.2.6-2.2.7) and for the lattice theories it is convenient to rewrite it as,

$$\frac{\partial(g^{-2})}{\partial(ln\, a)} = -2\beta_0 - 2\beta_1 g^2 + \cdots . \qquad (4.1.1)$$

There are two possible reasons for the exact β-function to disagree with the above perturbative result in a region away from the fixed point at $g_{bare}=0$. The first one is that, since the expansion parameter g_{bare} is large, there are higher order perturbative corrections to the 2-loop result. The more important cause is the non-perturbative one and depends on the topology of the group, the presence of non-trivial phase structure and a significant contribution from the irrelevant lattice operators. There are several approximate ways of mapping the phase structure in the extended coupling constant space (Monte-Carlo, mean field, strong coupling, ...) in certain regions, but none of them provides a clue as to the quantitative size of the non-perturbative effects. In this respect MCRG is unique. By calculating the non-perturbative β-function we not only know the corrections, but we also define what the scaling behaviour should be at large g_{bare}.

Eq.(4.1.1) shows that near $g_{bare}=0$ the rate of change of g^{-2} is essentially a constant and given by, $2\beta_0$. For SU(2), the bare charge in the $[K_F, K_A]$ action

space is given by,

$$K \equiv \frac{4}{g^2_{bare}} \;=\; K_F + \frac{8}{3} K_A \;. \tag{4.1.2}$$

Then integrating Eq.(4.1.1) one gets [1],

$$\Lambda_L \, a \underset{a \to 0}{\sim} \left[\frac{6\pi^2}{11} K\right]^{\frac{51}{121}} \exp\left[-\frac{3\pi^2}{11} K + \frac{10\pi^2}{11} \frac{K_A}{K}\right] , \tag{4.1.3}$$

where Λ_L is the renormalisation group invariant mass-scale for the lattice regularisation scheme. For the SU(3) theory, the analogous 2-loop result for points on the Wilson axis is,

$$\Lambda_L \, a \underset{a \to 0}{\sim} \left[\frac{8\pi^2}{33} K_F\right]^{\frac{51}{121}} \exp\left[-\frac{4\pi^2}{33} K_F\right] . \tag{4.1.4}$$

In a lattice calculation, any physical quantity with dimensions of mass, m, is calculated in units of the lattice spacing a; i.e., one measures ma. If the continuum limit is taken keeping m constant, then ma varies as,

$$ma \;=\; (const.)\, f\,(g_{bare}) \;, \tag{4.1.5}$$

where the scaling function $f\,(g_{bare})$ goes to zero in a well-defined manner as $g_{bare} \to 0$. The statement of scaling is that the function $f\,(g_{bare})$ be the same for all dimensionful physically measurable quantities. It is only in such a scaling region that one can define a universal β-function. If different physical quantities scale differently in a given region, the results are not likely to have much relevance to the continuum behaviour of the theory. For example, in the strong coupling limit, both the string tension σa^2 and the mass gap ma behave like $ln\,(g^2)$, and therefore the "β-functions" for the two quantities differ by a factor of 2.

The statement of asymptotic scaling is that the measured $f\,(g_{bare})$ be the same as the right-hand side of Eqs.(4.1.3-4.1.4). For example, when the

logarithm of the string tension is plotted as a function of g^{-2}, then the asymptotic slope of the curve is expected to be $-1/\beta_0$. Therefore, in order to expect asymptotic scaling, the first term in Eq.(4.1.1) should dominate even at $g_{bare} \sim 1$. This is not necessarily true in a real theory. For instance, it is known that for the SU(2) theory, Eq.(4.1.3) is not obeyed near the crossover region, when K_A is not very small [1]. However, as shown by Grossman and Samuel using large N resummation of the perturbation theory [2], it is possible to find a scaling function, which agrees well with the Monte-Carlo data of Ref.[1]. It is,

$$\Lambda_L \, a \underset{a \to 0}{\sim} \left[\frac{6\pi^2}{11} K_{eff} \right]^{\frac{51}{121}} \exp\left[-\frac{3\pi^2}{11} K_{eff} \right] , \tag{4.1.6}$$

where K_{eff} satisfies,

$$K_{eff} = K_F + \frac{8}{3} K_A - \frac{10}{3} \frac{K_A}{K_{eff}} . \tag{4.1.7}$$

Since for small K_A, the Eqs.(4.1.6-4.1.7) do reproduce Eq.(4.1.3), we have here an example, where there is scaling but not asymptotic scaling.

In our calculation of the non-perturbative β-function we measure deviations from the 2-loop result and determine what the true scaling behaviour should be. Such a measurement can be used to check for any phase structure in the lattice theory and to determine the region of asymptotic scaling. The measured $\Delta\beta$ (see Eq.(3.2.6)) is shown in Figs. 4.1 and 4.2 and is to be used as follows : The change in the lattice mass between $K_F - \Delta K_F$ and K_F, with ΔK_F evaluated at K_F, should be $\sqrt{3}$. This independence from perturbative results is essential since we do observe significant deviations from it.

Finite Size Effects

A word about finite size effects is necessary, since the numerical simulations are done on a finite size lattice. In addition to taking the continuum limit, one has to also take the limit where this infrared cut-off goes to zero. In real calculations the ultraviolet and the infrared cut-offs are separated by only an order of magnitude, and hence an unambiguous statement about scaling can be made only when one has understood how the finite size of the lattice has affected the results.

In finite temperature field theories, the temperature acts as an infrared cut-off on the theory. It is known that the counter-terms needed to regularise the theory at the ultraviolet end are the same for both $T=0$ and $T\neq 0$ [3]. The perturbative β-function can be defined, for example in the minimal subtraction scheme [4], such that it depends only on the singular behaviour of the theory. Therefore, though there are finite corrections to various physical quantities at $T\neq 0$, the perturbative β-function can be defined to be the same as the one for $T=0$.

In an MCRG calculation, the finite size effects inevitably change the measured expectation values because of the creation of interactions of longer range than the lattice size. These effects are more visible on the smaller blocked lattices. An attempt to get rid of these effects on a quantity such as like the β-function is made by comparing the expectation values only on the lattices having the same size and the same boundary conditions. Suppose that the two starting points $\{K^A\}$ and $\{K^B\}$ happen to lie on the same flow line. Then the two actions will be the same at every stage of matching. Though the expectation values will not be the same as the ones measured on an infinite lattice, they will be affected in the same manner by the finite size effects, and the β-function measured on a finite lattice will be the same as the one measured on an infinite

lattice.

In practice, however, the two starting points $\{K^A\}$ and $\{K^B\}$ do not lie on the same flow line. Hence a finite number of blocking steps cannot make the blocked actions on the two lattices exactly the same. The attractive nature of the RT makes the two actions $\{K^A\}$ and $\{K^B\}$ come close together (see Fig. 3.5), but since the flow lines cannot intersect, it is only in the limit of an infinite number of blocking steps that the two blocked actions become identical. The infrared cut-off independent β-function is thus defined as the one corresponding to the matching of the long distance behaviour of the two theories.

With a finite number of blocking steps, the residual finite size effects are a consequence of incomplete convergence to the RT. As pointed out by Wilson [5], these residual finite size effects decrease rapidly as one approaches the RT. For a fixed infrared cut-off, these residual effects vanish as the ultraviolet cut-off $\Lambda \to \infty$; i.e., when one can iterate the blocking process indefinitely. The renormalisation process removes all the divergent part of the ultraviolet cut-off dependence. Hence, these residual effects can be interpreted as the finite parts of the regulated integrals, which vanish in the limit $\Lambda \to \infty$. For the pure gauge theory, the ultraviolet divergence is logarithmic and the non-divergent cut-off dependent terms vanish like $O(\frac{1}{\Lambda^2})$. Thus in the perturbative region, a blocking by a scale factor b reduces the finite size effects by a factor b^2. In a region away from the fixed point, however, the finite size effects depend on how rapidly one converges to the RT, and this has to be numerically investigated by studying the non-leading eigenvalues of the linearised transformation matrix $T_{\alpha\beta}$. In practice, however, one can safely assume that the finite size effects are negligible when the matching process works at two different levels of blocking simultaneously; i.e., when the convergence to the RT is complete within statistical errors.

4.2 : Lattice Parameters and Statistics

The lattice size has to be an integer power of the scale factor times a constant. So we selected the two lattice sizes to be 9^4 and $(3\sqrt{3})^4$ on the basis of the available amount of computer time and the preliminary result of Wilson [5] on an 8^4 lattice. He found that the expectation value of the simple plaquette on the 1^4 lattice was adequate to establish a matching of the blocked actions. The reason for accepting matching on the basis of a single operator is that the theory is expected to have only one relevant coupling. We shall provide a posteriori evidence for this in the data. However, we did calculate a number of operators. They were :

(a) the simple plaquette,

(b) the 6-link rectangular ($6p$), L-shaped ($6l$) and twisted loops ($6t$),

(c) the $J=1$, $J=3/2$ and $J=2$ representations of the simple plaquette for SU(2), and the 6, 8, 10, 15, and 15' representations of the simple plaquette for SU(3).

The crossover from strong to weak coupling for a given size Wilson loop is a function of the coupling. This change is very sharp for non-abelian gauge theories and the larger loops exhibit the change at smaller values of g_{bare}. One can therefore achieve maximum sensitivity in the matching by using operators whose block expectation values are in the crossover region. Also since the ideal β-function is measured along the RT, the operators which are used in the matching process should have maximum projection along the RT, and as little contamination as possible from the irrelevant lattice operators. In principle this can be achieved by finding the eigen-vectors of the transformation matrix $T_{\alpha\beta}$, and in absence of any such information the perturbative results can be a good guide [6]. We evaluated small loops only because we expected a matching on the 1^4 and may be on a $(\sqrt{3})^4$ lattice. The higher dimensional representations were

selected to check if they are important in the renormalised action.

SU(2) :

The action for the SU(2) lattice gauge theory in the $[K_F, K_A, K_{3/2}, K_{6p}, K_{6l}, K_{6t}]$ space is defined in terms of the plaquette variables U_p and the three 6-link loops $(6p, 6l, 6t)$ as,

$$S = K_F \sum Tr U_p + K_{6p} \sum Tr U_{6p} + K_{6l} \sum Tr U_{6l} + K_{6t} \sum Tr U_{6t}$$
$$+ K_A \sum [\frac{4}{3}(Tr U_p)^2 - \frac{1}{3}] + K_{3/2} \sum [2(Tr U_p)^3 - Tr U_p] . \qquad (4.2.1)$$

Here all traces are normalised to unity and the sums are taken over all sites and positive orientations of the loops.

We decided to investigate the theory along

(i) the Wilson axis, where most of the Monte-Carlo calculations have been performed, and

(ii) the Migdal-Kadanoff improved action line (called M-K from here on) defined by, $K_A = -0.24 K_F$ [6], since at large g_{bare} there is evidence for it to be attractive and universal.

The range of couplings investigated along these lines was determined from the point of calculational efficiency. The limitation at larger g_{bare} is that the block expectation values become very small since the action evolves beyond the crossover into the strong coupling region. Consequently, to obtain a reliable matching, a very large statistical sample is required. At weaker g_{bare}, the starting action is not very close to the RT and a reliable matching cannot be done. Also the critical slowing down makes the statistics worse. We therefore restricted ourselves to the intermediate coupling region. The expectation values on the blocked lattices were then near their crossover region, increasing the sensitivity

of the matching to a change in K_F.

The update was done using the Metropolis algorithm [7] in which the link to be updated was selected at random. At each link update 5 hits were made. The matrices were expressed as

$$U = a_0 + i a_j \sigma_j \tag{4.2.2}$$

and the 4 real numbers a_i were stored. For the full group update the hit matrices were constructed by choosing a_0 uniformly in a range $[1,1-\delta]$ and then the a_i were chosen uniformly on a sphere of radius $\sqrt{(1-a_0^2)}$. The value of δ was selected to give an acceptance rate of < 50%. In case of the icosahedral subgroup one of the 12 elements closest to the identity was used as a hit matrix. To decrease the effects of statistical correlation of data, we calculated the observables after every 5 sweeps. Also, all possible 3^4 (9 such), $(\sqrt{3})^4$ (81 such) and 1^4 (729 such) lattices were constructed. Even though the variables on these are correlated, we found that there still is a large increase in the statistics for a small increase in the CPU time. Two tests were made to check if the data were statistically independent. One was to divide the data into bins of 100 configurations each and calculate the errors from the binned data. The other was to calculate the auto-correlation coefficients C_γ,

$$C_\gamma = \frac{<\Omega(i)\Omega(i+\gamma)>}{<\Omega(i)\Omega(i)>}, \tag{4.2.3}$$

and define the auto-correlation length γ by C_γ=0.1. This provides more information than averaging successive pairs of data points until the standard deviation begins to fall by a factor of $\sqrt{2}$.

The first 2500 sweeps on each 9^4 lattice and the first 2000 sweeps on each $(3\sqrt{3})^4$ lattice were discarded to ensure thermalisation. The data sample was 1000 to 2500 configurations on the 9^4 lattices and 2000 to 4000 on the $(3\sqrt{3})^4$

lattices.

SU(3) :

The action for the SU(3) lattice gauge theory in the $[K_F, K_6, K_A, K_{6p}, K_{6l}, K_{6t}]$ space is defined to be,

$$S = \mathrm{Re}\,[\, K_F \sum Tr U_p + K_{6p} \sum Tr U_{6p} + K_{6l} \sum Tr U_{6l} + K_{6t} \sum Tr U_{6t}$$

$$+ K_6 \sum [\frac{3}{2}(Tr U_p)^2 - \frac{1}{2} Tr U_p\,] + K_A \sum [\frac{9}{8} |\, Tr U_p\,|^2 - \frac{1}{8}]\,]\,. \qquad (4.2.4)$$

Again the traces are normalised to unity and the sums are taken over all sites and positive orientations of the loops.

We investigated this theory along the Wilson axis only, since most of the other Monte-Carlo calculations have been made along this line.

Once again the update was done using the Metropolis algorithm [7] in which the link to be updated was selected at random. At each link update 20 hits were made. The first 500 sweeps were discarded to ensure thermalisation. The data sample for the 9^4 lattices at K_F=6.5(7.0) consisted of 593 (560) configurations separated by 15 update sweeps. The configurations on the $(3\sqrt{3})^4$ lattices were separated by 10 update sweeps and their number varied between 650 and 1150.

4.3 : Analysis and Results for SU(2)

We first discuss the calculation in which the gauge group SU(2) was approximated by its icosahedral subgroup in order to reduce the computer time. The first possibility we tried was to choose the block variable U^1 to be one of the six paths that maximised $Tr\,(U^1 \sum_i U_i^\dagger)$. This is a decimation transformation and we found that for the points on the Wilson axis, the change ΔK_F for a scale change

of $\sqrt{3}$ was much larger than that predicted by Eq.(4.1.1). Also the difference increased with increasing K_F. This construction was thereafter rejected. Next we enlarged the group space available to U^1 to all the 120 elements. Even in this case the data showed very clearly that keeping the blocked variable within the icosahedral group led to rapid disordering. Finally, we allowed U^1 to take any value inside the full SU(2) group. In this last case, after a few blockings the averaged icosahedral subgroup matrices cover the full group; consequently, the memory of the original discrete elements is washed out.

We also compared the results of the full group versus the icosahedral subgroup update. The blocking was done using the full group for both the cases. We found that at K_F=5.2 on the M-K line the results were identical. Therefore, we continued to use the icosahedral update with the full group blocking because of a factor of ~3 in update speed.

The errors in most of the block variables were reduced to <1%, as shown in the example of matching the 9^4 lattice at K_F=4.0 with the $(3\sqrt{3})^4$ lattice at K_F=3.52 on the M-K line in Table 4.1. On the 1^4 lattices all the operators could not be matched simultaneously. On these lattices the 6-link operators are bigger than the lattice size and were found to be rather insensitive to changes in K_F. Also both the 6-link operators and the higher spin operators had larger errors. Therefore, the matching was done mainly on the basis of the simple plaquette in the fundamental and the adjoint representations. On the $(\sqrt{3})^4$ lattices, however, it was possible to match all the operators at the same time and therefore all of them were considered in the matching process. In most cases we could not simultaneously match observables on both the 1^4 and $(\sqrt{3})^4$ lattices and found a larger value of ΔK_F from matching on the $(\sqrt{3})^4$ lattice. At present we cannot isolate the errors due to residual finite size effects, incomplete convergence of actions and limited statistical accuracy. We therefore

estimate ΔK_F separately for the matching on the 1^4 and $(\sqrt{3})^4$ lattices. An interesting feature of our data is that the values of ΔK_F determined from matching on the $(3\sqrt{3})^4$ and $(\sqrt{3})^4$ lattices approach the limiting value from above, while those obtained from matching on the 3^4 and 1^4 lattices approach from below. This can be seen from the example in Table 4.1 by trying a gedanken calculation to obtain matchings at different levels. Such an effect is likely to be a result of the alternating boundary conditions in the blocking process; i.e., the first blocking rotates the blocked lattice with respect to the original lattice and the second blocking realigns the axes with those of the original lattice. Because of this we are able to see the convergence towards the limiting value of ΔK_F more clearly and the two sets of results should provide bounds on the actual value of ΔK_F. The results along the Wilson line using the 120 element subgroup update are shown in Fig. 4.1 and those along the M-K line obtained using the full group update are shown in Fig. 4.2.

Several noteworthy features of these results are :

(a) The ΔK_F along the Wilson axis dips well below the 2-loop value at K_F=2.5. When the Monte-Carlo results are combined with the β-function obtained in the strong coupling region[†] (see Fig. 4.3), the behaviour appears to be oscillatory. Such a behaviour can be understood in terms of the phase structure in the extended coupling constant space. As shown in Fig. 3.4, phase structures distort the RT flowing from the UVFP to the IRFP. If the phase structure repels the RT, then in the region BC, the flow along the RT gets sandwiched between two repelling regions and slows down. This results in a dip in the β-function. After passing the point B, however, the flow along RT speeds up, because it gets repelled by the phase structure and attracted by the IRFP. The result is a

[†] This was obtained from the results of [9] by imposing the condition that the physical string tension does not change when the lattice spacing a is changed.

bump in the β-function. Such a repelling phase structure is known to exist in the $[K_F, K_A]$ space (see Fig. 5.3) and has been interpreted as causing the crossover region at K_F=2.2 [10], characterised by a bump in the specific heat. As expected, the β-function in Fig. 4.3 does show a bump on the strong coupling side of this crossover region and a dip on the weak coupling side of it.

(b) For larger K_F on the Wilson axis, the measured ΔK_F is within ~10% agreement of the asymptotic scaling. However, the β-function seems to be rising above the 2-loop value up to K_F=3.5. In case of an incomplete convergence of the two starting actions $\{K^A\}$ and $\{K^B\}$, the ΔK_F obtained assuming that the matching takes place on the 1^4 lattice, is expected to be a lower bound for the limiting value [8]. An easy way to see this is to try shifting the trajectories in Fig. 3.5. Therefore, we are led to believe that there are substantial higher loop and non-perturbative corrections to the 2-loop result in the so-called weak coupling region. This implies that checks of QCD require a very careful calculation of the β-function to define scaling.

(c) There appears to be another smaller wiggle in the β-function around K_F~3.0 on the Wilson axis. It is within the error bars and therefore all by itself would not have been significant. But when combined with an independent measurement of the specific heat [11], which shows a smaller bump around K_F=2.55 (see Fig. 4.4), it implies the existence of another crossover region, though not as strong as the first one. Perhaps there are more such wiggles, smaller and smaller in size as one proceeds towards the fixed point, making the β-function look like a damped oscillator. Their decreasing size and increasing statistical errors due to critical slowing down make them invisible. Such a conclusion has indeed been arrived at by Caneschi, Halliday and Schwimmer [12]. They interpret the crossover region as the result of condensation of monopoles and closed loops of flux corresponding to the centre Z(2) of SU(2). The introduction of K_A

singles out such topological objects of the size of a plaquette. As the coupling becomes weaker, thicker loops and bigger topological objects can get formed, but the change will no longer be as drastic as the one the first time these objects appeared. Therefore the wiggles will get smaller. Another way of saying this is that, if one extends the action in the space of adjoint (and higher) representations of bigger loops, though the phase structures will extend out to larger K_F, they will be farther away from the Wilson axis.

(d) The above conclusion is rather drastic and if true will force us to review the standard approach to the continuum limit. Therefore, we need to make sure that these wiggles are not caused by some spurious effects. One of the probable cause of spurious effects is the deconfinement transition. This transition is second order in case of the SU(2) theory, and therefore slows down the motion through the phase space considerably. The order parameter for this transition is the expectation value of the Wilson line $<L>$; i.e., the path ordered product of link matrices closed by the periodic boundary conditions on the lattice. We monitored its absolute value and the results are shown as squares in Figs. 4.1 and 4.2. Near the transition the statistics become worse, and the discrepancy between the ΔK_F values determined from the matchings on the $(\sqrt{3})^4$ and the 1^4 lattices increases. However, $<|L|>$ does not show any rapid behaviour and some of the wiggles on the Wilson axis are even outside the region of transition. Also as will be seen in the next chapter, no wiggles are seen in the improved action determined using the same data sample. There the phase structure is avoided by going into a multi-dimensional coupling constant space. Therefore, it is likely that the wiggles are the result of working in a restricted coupling constant space.

(e) The ΔK_F along the M-K line does not show any obvious wiggles. There is a rise in ΔK_F at K_F=3.1, which can be interpreted as caused by the strong

coupling effects. Since the M-K line lies farther away from the phase structure, these results support our previous claim that the wiggles are caused by the phase structure in the extended coupling constant space. The discrepancy between the ΔK_F values determined from the matchings on the $(\sqrt{3})^4$ and the 1^4 lattices increases for K_F>4.0. This is the combined effect of the incomplete convergence to the RT and poorer statistics due to critical slowing down. Even at the largest value of K_F that we have worked with, the agreement with the asymptotic scaling is not good. This is not unexpected since K_A is large in this region. However, the most interesting feature is that the results agree very well with those predicted by Grossman and Samuel (cf. Eqs.(4.1.6-4.1.7)), throughout the range of couplings investigated. This whole analysis implies that the non-perturbative effects caused by the phase structures can be highly reduced and scaling observed, by choosing an appropriate action to work with.

As a final check, we are currently running the programmes on an 18^4 lattice using the new 64 node concurrent processor constructed at Caltech. If the wiggles do not move and the results agree with those obtained on a 9^4 lattice here, it would imply that the non-perturbative behaviour is not caused by finite size effects and an improved action approach is needed to see the scaling behaviour.

We also calculated the eigenvalues of the linearised transformation matrix, $T_{\alpha\beta}$, using 1280 configurations at K_F=5.05 on the M-K line. When only the $[K_F\ ,\ K_A]$ operators were used, the leading eigenvalue was 1.04, 0.92 and 0.93 at the 2^{nd}, 3^{rd} and 4^{th} blocking, respectively. The non-leading eigenvalue was less than 0.1 at all the three stages. In the $[K_F\ ,\ K_A\ ,\ K_{6p}]$ space the leading eigenvalue was 0.92, 0.79, and 1.16 at the 2^{nd}, 3^{rd} and 4^{th} blocking, respectively. The non-leading eigenvalue was smaller than 0.4 at all the three steps. Though limited statistics restricted us from enlarging the space any further, these results provide a good check on the efficiency of the $\sqrt{3}$ blocking

transformation. In particular, we can see that the RT is more attractive in the directions representing the higher representation operators, than in the directions representing the 6-link operators.

4.4 : Results for SU(3)

The results for ΔK_F have been obtained at K_F=6.5 and 7.0 along the Wilson axis. The block variables from the 9^4 starting lattice at K_F=7.0 were compared with those from the $(3\sqrt{3})^4$ starting lattices at K_F=6.51 and 6.54. The block variables from the $(3\sqrt{3})^4$ starting lattices at K_F=6.03 and 6.06 provided upper and lower bounds for the 9^4 starting lattice at K_F=6.5 as shown in Table 4.2. As was the case in SU(2), here also the convergence towards the limiting value of ΔK_F showed an alternating behaviour. The values of ΔK_F determined by linear interpolation are,

$$\Delta K_F = 0.48\pm0.02 \; : \; K_F=7.0 \; , \tag{4.4.1}$$

$$\Delta K_F = 0.46\pm0.01 \; : \; K_F=6.5 \; . \tag{4.4.2}$$

The corresponding 2-loop perturbative results are 0.484 and 0.487, respectively. As expected, the phase structure in the extended coupling constant space causes the β-function to dip below the perturbative result on the weak coupling side of the crossover region. It remains to be checked whether or not more wiggles occur for still weaker couplings.

There were two very significant differences between SU(2) and SU(3). The auto-correlation length γ for the block variables on the 1^4 lattices (defined by C_γ=0.1) was ~3–4. This is a factor of ~5 smaller than the SU(2) value. The more important difference was the vastly improved quality of matching for SU(3). The variables on the 1^4 and the $(\sqrt{3})^4$ lattices could be simultaneously matched and even the variables on the 3^4 lattices showed rough agreement.

This implies that for SU(3), the RT is reached approximately after one blocking transformation starting from the simple plaquette action. The improved action analysis in the next chapter also arrives at the same conclusion.

REFERENCES

[1] G. Bhanot and R. Dashen, Phys. Lett. 113B (1982) 299.

[2] B. Grossman and S. Samuel, Phys. Lett. 120B (1983) 383.

[3] S. Weinberg, Phys. Rev. D9 (1974) 3357.

[4] G. 'tHooft and M. Veltman, Nucl. Phys. B44 (1972) 189.

[5] K. Wilson, in *Recent Developments in Gauge Theories* (Cargese 1979), ed. G. 't Hooft et al, Plenum Press, New York (1980).

[6] K. M. Bitar, S. Gottlieb and C. Zachos, Phys. Rev D26 (1982) 2853.

[7] N. Metropolis et. al., J. Chem. Phys. 21 (1953) 1087.

[8] A. Hasenfratz, P. Hasenfratz, U. Heller and F. Karsch, CERN preprint, CERN-TH-3818 (1984).

[9] J. M. Drouffe and J. B. Zuber, Phys. Rep. 102 (1984) 1.

[10] G. Bhanot and M. Creutz, Phys. Rev. D24 (1981) 3212.

[11] M. Grady, Los Alamos preprint, LA-UR-83-3223 (1983).

[12] L. Caneschi, I. G. Halliday and A. Schwimmer, Nucl. Phys. B200 [FS4] (1982) 409.

FIGURE CAPTIONS AND FIGURES

[4.1]ΔK_F along the Wilson axis for the SU(2) theory. The crosses are based on the matching on the 1^4 lattice, while the circles are for the matching on the $(\sqrt{3})^4$ lattice. The dashed line is the 2-loop perturbative result. Also shown as squares are the expectation values of the absolute magnitude of the Wilson line. Their errors are smaller than the size of the squares.

[4.2]ΔK_F along the M-K line for the SU(2) theory. The crosses are based on the matching on the 1^4 lattice, while the circles are for the matching on the $(\sqrt{3})^4$ lattice. The dashed line is the 2-loop perturbative result. The dotted line is the result of Grossman and Samuel. Also shown as squares are the expectation values of the absolute magnitude of the Wilson line. Their errors are smaller than the size of the squares.

[4.3]The Monte-Carlo results combined with the strong coupling ones for ΔK_F along the Wilson axis for the SU(2) theory.

[4.4]The specific heat for the SU(2) theory measured along the Wilson axis. This figure is taken from Ref.[9].

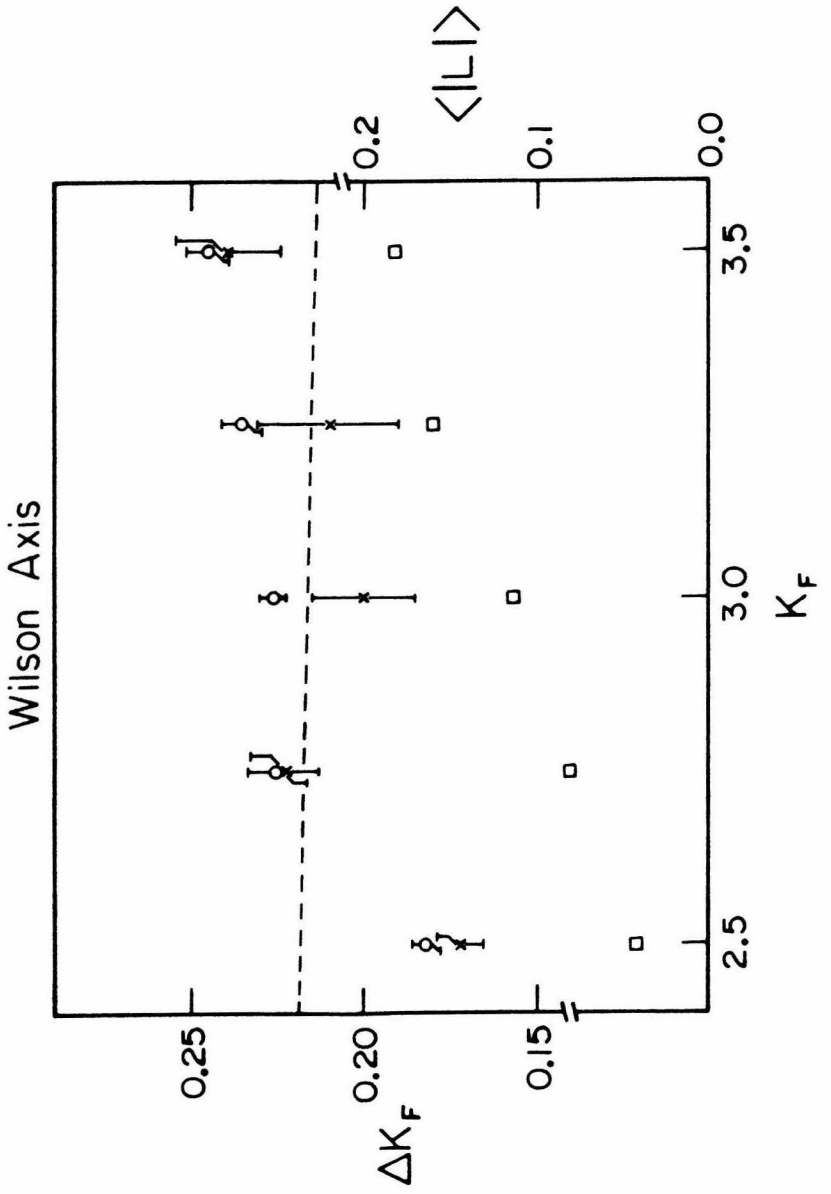
Wilson Axis
0.25
0.20
0.15
ΔK_F
2.5
3.0
3.5
K_F
0.2
0.1
0.0
$\langle |L| \rangle$

Fig. 4.1

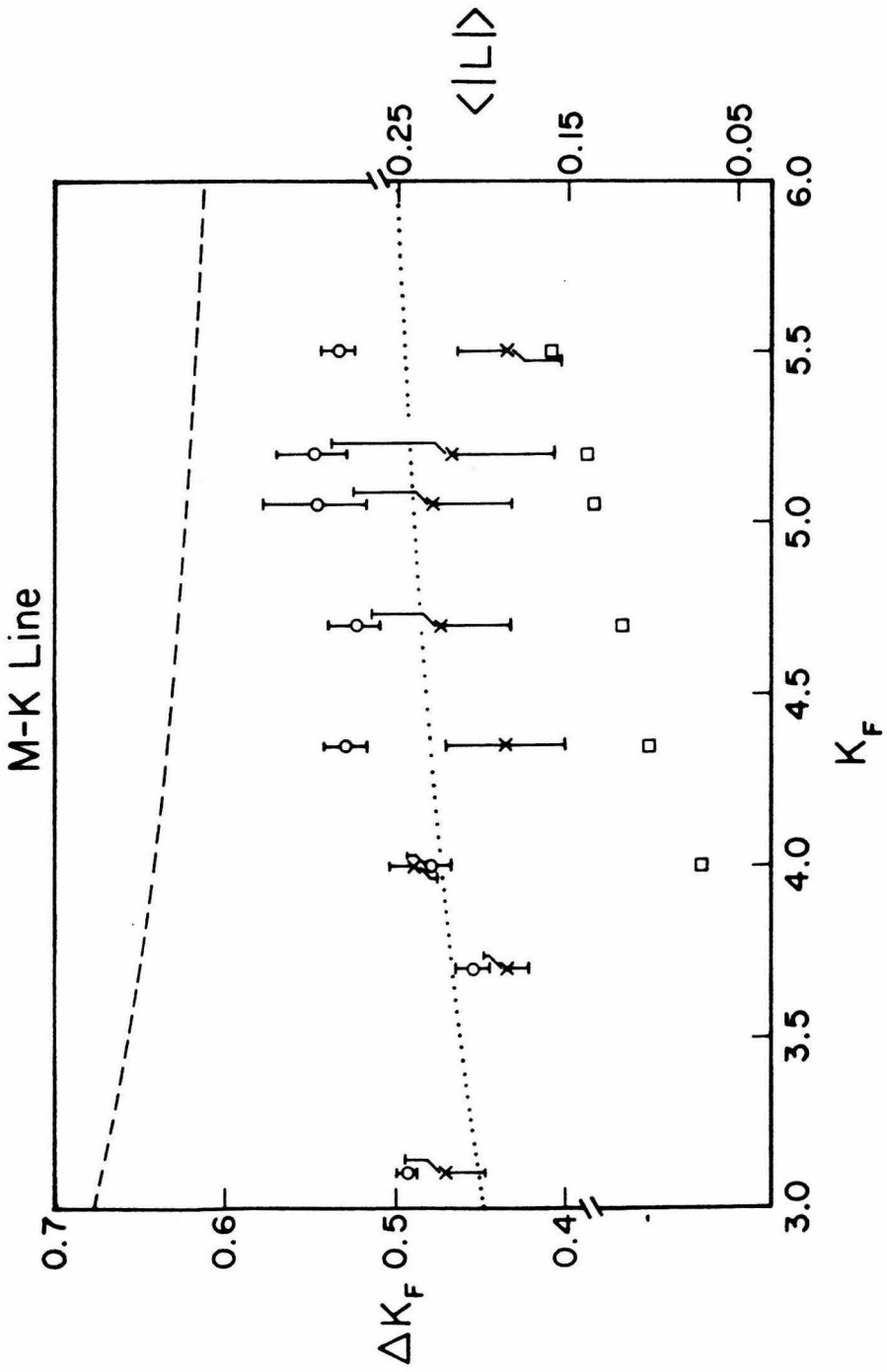

Fig. 4.2

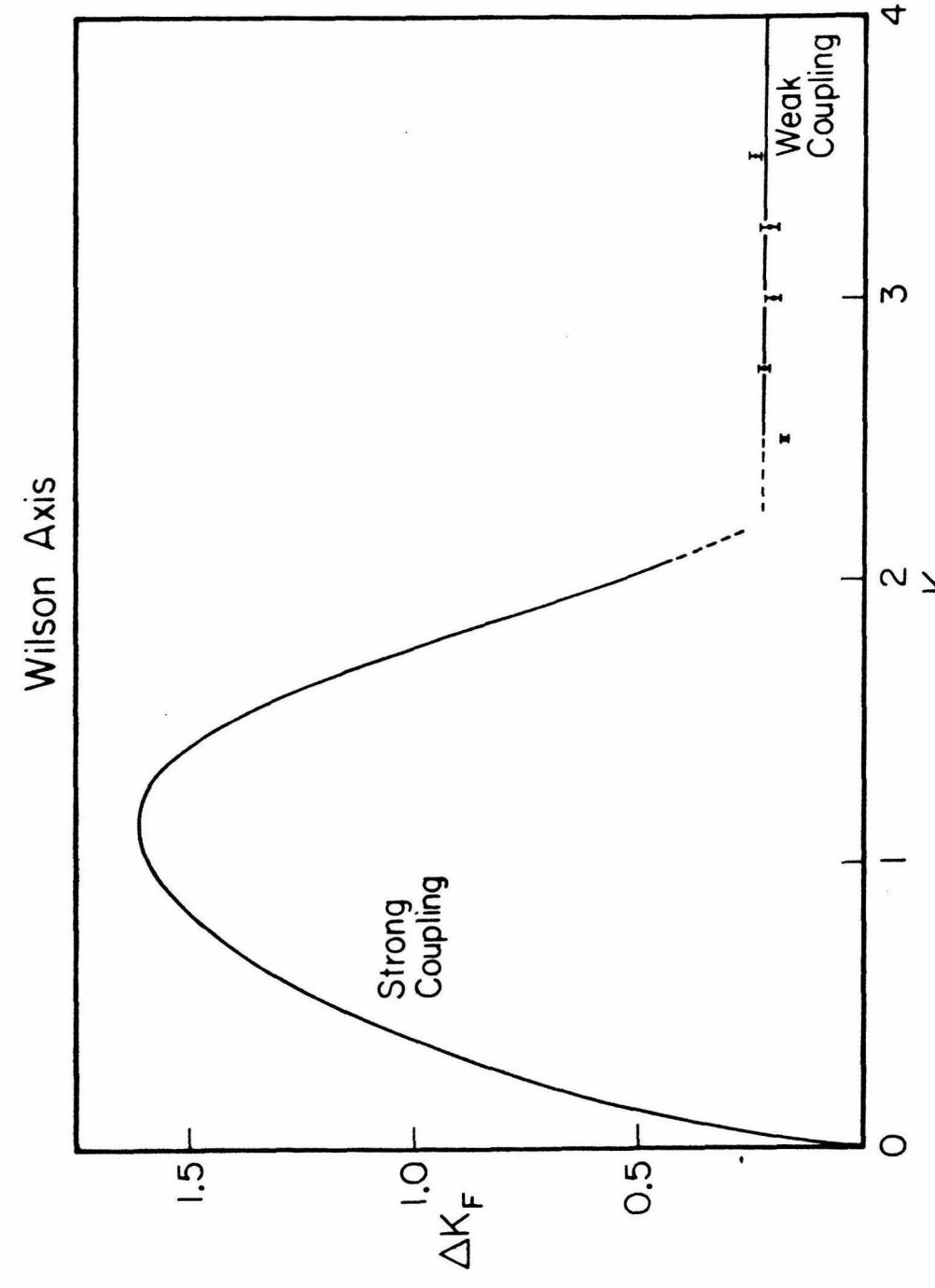
Wilson Axis
Strong Coupling
Weak Coupling
1.5
1.0
0.5
ΔK_F
0
1
2
3
4
K_F

Fig. 4.3

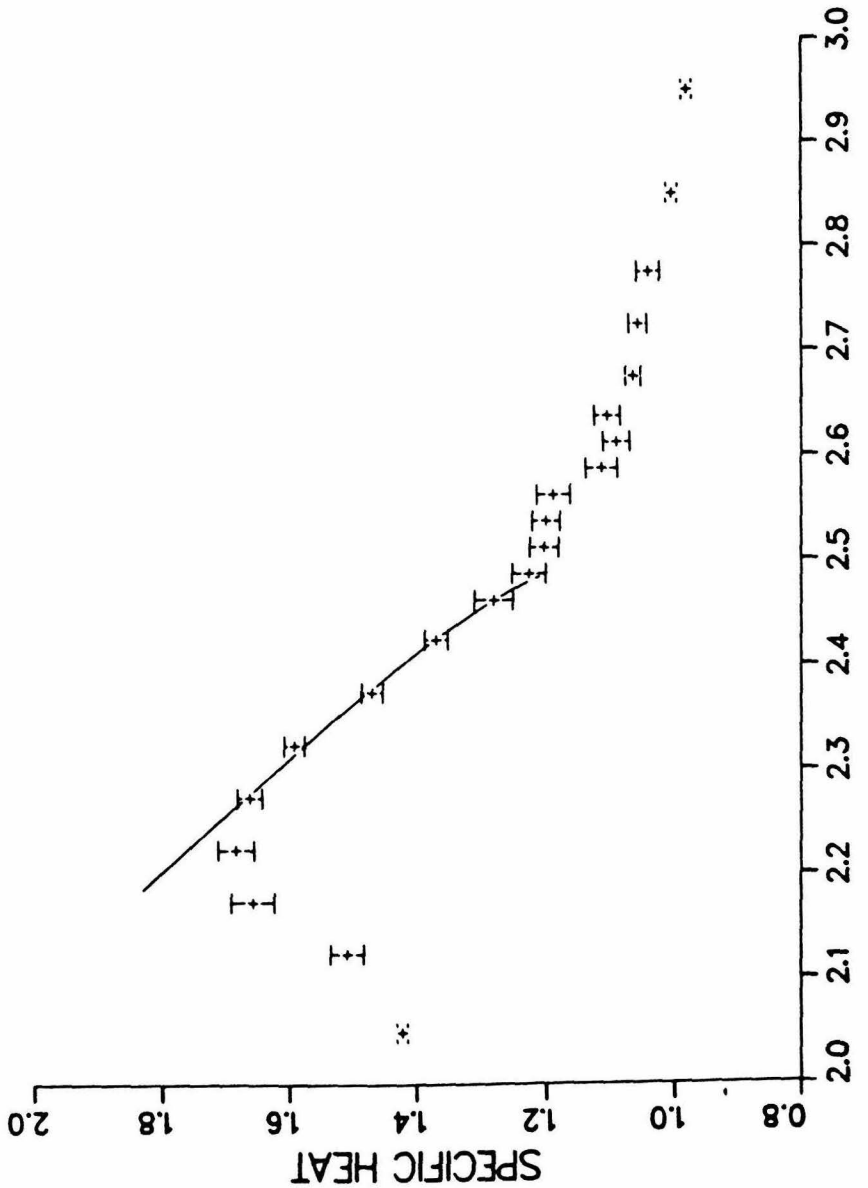
SPECIFIC HEAT
0.8
1.0
1.2
1.4
1.6
1.8
2.0
2.0
2.1
2.2
2.3
2.4
2.5
2.6
2.7
2.8
2.9
3.0
K_F

Fig. 4.4

TABLES

9^4 LATTICE K_F = 4.0 K_A = -0.96						
Latt size	Fund	6p	6l	6t	Adj	J=3/2
9	.6796(00)	.4974(001)	.5305(01)	.4933(001)	.3519(01)	.1341(01)
$3\sqrt{3}$	.6027(02)	.3816(004)	.4498(03)	.4303(003)	.2607(03)	.0814(02)
3	.5479(06)	.3170(009)	.3828(09)	.3586(010)	.2033(06)	.0518(03)
$\sqrt{3}$	.4673(27)	.2418(038)	.3064(31)	.2978(034)	.1345(20)	.0243(06)
1	.5889(51)	.5748(114)	.4957(57)	.4858(168)	.3105(53)	.1745(41)
$(3\sqrt{3})^4$ LATTICE K_F = 3.52 K_A = -0.8448						
Latt size	Fund	6p	6l	6t	Adj	J=3/2
$3\sqrt{3}$	.6436(01)	.4472(02)	.4815(02)	.4408(02)	.3032(01)	.0993(01)
3	.5416(05)	.3112(07)	.3775(06)	.3569(07)	.1983(05)	.0499(02)
$\sqrt{3}$	.4672(18)	.2391(24)	.3052(21)	.2967(25)	.1355(13)	.0255(05)
1	.5913(41)	.5548(36)	.4916(36)	.4576(63)	.3169(42)	.1817(31)

Table 4.1 : The expectation values of operators on the 9^4 lattice and blocked lattices at K_F=4.0 on the M-K line. The matching coupling on the $(3\sqrt{3})^4$ lattice was K_F=3.52 on the M-K line. The data sample consisted of 1500 configurations on the 9^4 lattice and 3000 configurations on the $(3\sqrt{3})^4$ lattice. The statistical errors are shown in parentheses.

Lattice Size	Operator	$(3\sqrt{3})^4$ lattice K_F=6.03	9^4 lattice K_F=6.5	$(3\sqrt{3})^4$ lattice K_F=6.06
9^4	plaq		0.6385(1)	
	6p		0.4435(2)	
	6l		0.4777(2)	
	6t		0.4385(2)	
	6		0.3312(2)	
	8		0.3690(2)	
	10		0.1418(2)	
$(3\sqrt{3})^4$	plaq	0.5986(5)	0.5518(4)	0.6018(4)
	6p	0.3907(7)	0.3230(6)	0.3952(5)
	6l	0.4256(7)	0.3915(5)	0.4297(5)
	6t	0.3832(8)	0.3718(6)	0.3875(6)
	6	0.2847(6)	0.2278(5)	0.2884(4)
	8	0.3216(6)	0.2639(5)	0.3253(5)
	10	0.1101(4)	0.0709(3)	0.1126(3)
3^4	plaq	0.4845(13)	0.4928(09)	0.4900(09)
	6p	0.2512(15)	0.2586(12)	0.2575(11)
	6l	0.3164(14)	0.3235(11)	0.3226(10)
	6t	0.2962(15)	0.2998(12)	0.3027(11)
	6	0.1662(11)	0.1718(08)	0.1708(08)
	8	0.1983(11)	0.2047(09)	0.2033(08)
	10	0.0410(05)	0.0427(04)	0.0430(04)
$(\sqrt{3})^4$	plaq	0.4041(28)	0.4064(24)	0.4147(21)
	6p	0.1804(29)	0.1833(26)	0.1906(22)
	6l	0.2404(30)	0.2445(25)	0.2514(22)
	6t	0.2279(32)	0.2336(27)	0.2394(24)
	6	0.1063(18)	0.1069(15)	0.1132(14)
	8	0.1326(20)	0.1333(17)	0.1403(15)
	10	0.0186(06)	0.0185(05)	0.0208(05)
1^4	plaq	0.4607(61)	0.4695(60)	0.4806(45)
	6p	0.3765(40)	0.3885(42)	0.3853(33)
	6l	0.3401(52)	0.3500(50)	0.3569(40)
	6t	0.3077(64)	0.3256(70)	0.3171(52)
	6	0.1790(48)	0.1839(46)	0.1948(38)
	8	0.2011(53)	0.2071(50)	0.2184(41)
	10	0.0703(27)	0.0718(26)	0.0788(22)

Table 4.2 : The matching of expectation values for K_F=6.5 on the Wilson axis for the SU(3) theory. The statistical errors are shown in parentheses.

Chapter 5

IMPROVING THE ACTION

5.1 : Various approaches to improvement

In present Monte-Carlo simulations, the size of the lattice one can work with is limited by the available computer power. Since one does not have any systematic way of estimating the finite size effects in such calculations, one needs to ensure the condition $\xi \ll L$. Then because of the fact that the value of $\frac{L}{a}$ is limited by the computer capabilities, one is forced to choose $\xi \sim a$. When one works with the simple plaquette action, this gives rise to serious finite spacing effects; i.e., the bare coupling is too large and one is working with an action far from the continuum limit. There is a rapid crossover from the strong coupling to the weak coupling behaviour which shows up as a sharp bump in the specific heat. Beyond this bump, the range of couplings one can explore, while maintaining $\xi \ll L$, is very small. The objective of improving the action is to modify the action such that, even though $\xi \sim a$, the extrapolation to the continuum is smoother. In such a case, the bump in the specific heat becomes less pronounced and moves towards the strong coupling region; i.e., the roughening transition occurs for a smaller value of $\frac{\xi}{a}$. Hence the range of couplings one can use to check scaling increases. It should be noted that though g_{bare} is still too large in this region, the mass ratios are likely to be close to their continuum values. The absolute scale can then be fixed using the non-perturbative β-function, which can be numerically measured independent of the finite size effects.

To find an action which is close to the continuum limit, one needs to remove the effects of irrelevant lattice operators (the ones which vanish as the continuum limit is taken). Since the choice of the lattice action is not unique, namely, Wilson loops of different shapes and sizes can be used as the action which becomes $F_{\mu\nu}F^{\mu\nu}$ in the continuum limit, a suitable linear combination of the Wilson loops can produce an action which is less contaminated by the irrelevant operators. If this is systematically done, then even though $\xi \sim a$, the action can be very close to the continuum limit. The fact that we are working with large g_{bare} means that we are effectively trying to simulate the long distance behaviour of the theory. This can be implemented making use of the theory of Renormalisation Group. Several approaches exist in the literature. Outstanding amongst them are the Migdal-Kadanoff approximate renormalisation scheme, Symanzik's perturbative improvement programme and the Monte-Carlo Renormalisation Group, which is the subject of study here. Before we discuss these different techniques, let us note some important points :

(a) The shape of the renormalised trajectory depends on the renormalisation group transformation used for integrating out the short distance behaviour of the theory and obtaining the effective long range interaction. So the different schemes may give rise to different trajectories along which the continuum limit would be smoother.

(b) On the lattice, the set of all Wilson loops is overclosed; i.e., the number of Wilson loops is much larger than the number of irrelevant lattice operators. Therefore, to eliminate the effect of irrelevant lattice operators, one does not have to work with all possible Wilson loops. A linearly independent subset will do. For instance, it has been shown in all orders of perturbation theory [1] that, out of the three 6-link Wilson loops, only two are linearly independent. The coefficient of the L-shaped loop can be set to zero,

without loss of generality.

(c) The simple plaquette action satisfies physical positivity of the transfer matrix. But when operators of dimension 6 or higher are added to it, the physical positivity of the theory is lost in general. This occurs because the new terms couple link variables separated by more than one lattice spacing. It is still possible to define the transfer matrix [2]. But the occurrence of complex eigenvalues gives rise to damped oscillatory behaviour of the correlation functions, and the spectral decomposition of two-point functions gets contributions with negative weight. However, it can be shown that the positivity is lost only at energies of the order of the cut-off [2]. The effect becomes unimportant at weak couplings, and the positivity is restored in the continuum limit.

Migdal-Kadanoff Approximate Renormalisation

Let us start with the single plaquette action on the original lattice,

$$e^{\sum_{plaq} A_{plaq}(U_{plaq};a)} = exp\Big[\sum_{r,plaq} \frac{1}{d_r} K_r \, \chi_r(U_{plaq};a) \Big] , \qquad (5.1.1)$$

where, $\chi_r(U)$ is the trace of U in the irreducible representation r of the group, and $d_r \equiv \chi_r(1)$ is the dimensionality of the representation. The gauge invariant action is a class function; i.e., it does not depend on the degrees of freedom which can be gauged away. The set of all characters forms a complete orthogonal basis for a "Fourier" series expansion of any class function,

$$e^{A_{plaq}(U;a)} = \sum_r F_r(a) \, d_r \, \chi_r(U) . \qquad (5.1.2)$$

The orthogonality relation for the characters can be used to invert this expression and obtain $F_r(a)$ in terms of the single plaquette action.

To obtain the effective action at larger scales, $A(U;\lambda a)$, we have to perform the group integration over an appropriate set of links. In general, such an integration of short distance behaviour of the theory causes all types of gauge invariant loops to appear in the new action. However, for 2-dim gauge theories, the integration over alternate lines of links can be carried out exactly, resulting in a recursion relation between $F_r(\lambda a)$ and $F_r(a)$ [3,4]. The new action is then restricted to the space of single plaquettes. In higher dimensions, it is not possible to carry out an exact integration because of the interactions of the links in the directions transverse to the plane of decimation. But an approximate result can be obtained by moving these transverse interactions to neighbouring planes and then performing the same integrations as in the 2-dim case. Migdal's scheme [3] corresponds to first moving the plaquette interactions so that the orthogonal planes do not have any links in common, performing the integration over alternate lines of links in all directions, and then recombining the split plaquette interactions on the blocked lattice (Fig. 5.1). Kadanoff's scheme [4] corresponds to moving either the transverse or the longitudinal interactions so as to decouple them and then performing the integration over alternate links. Also the procedure is carried out over all the directions in succession (Figs. 5.2 and 5.3). Both these approximations can be described by a single generalised recursion relation,

$$e^{A_{plaq}(U;\lambda a)} = [\ \sum_r \{ \frac{1}{d_r} \int dV\, e^{A_{plaq}(V;a)\lambda^b} \chi_r^*(V) \}^{\lambda^2}\, d_r \chi_r(U)\ ]^{\lambda^{d-2-b}} \quad . \quad (5.1.3)$$

Migdal's result corresponds to $b=0$ [3] and Kadanoff's result corresponds to $b=2$ [4]. It is worth noting that when the above result is analytically continued to the case of infinitesimal scale change, $\lambda=1+\varepsilon$, the dependence on b disappears and both the schemes become identical [5].

The projection of the effective action generated by a renormalisation group transformation on the space of single plaquette actions is a rather crude approximation. It works well in the strong coupling region [4], because there $\xi<a$ and long range interactions contribute very little. But in the weak coupling region the recursion relation fails to produce the correct β-function. On the contrary, only the numerical coefficients of the β-function turn out to be wrong and the property of asymptotic freedom is maintained [3]. In other applications, this approximation misses the order and the critical exponents of the phase transitions, but still succeeds in finding the critical couplings to a good accuracy [3,4,6].

The phase diagram of the $SU(2)$ lattice gauge theory in the space of single plaquette actions has been studied by numerically iterating the recursion relation [6]. The amazing agreement of these results with the Monte-Carlo data [7] implies that this method might provide a good estimate for the renormalised trajectory. Indeed Bitar, Gottlieb and Zachos [6] did find a trajectory to which all the renormalisation flows converged (see Fig. 5.4). It is roughly described by,

$$K_A = -0.24\, K_F \ , \ K_{3/2} = 0.12\, K_F \ , \tag{5.1.4}$$

in the region, $1<K_F<4$. The important result here is that the trajectory moves off into the negative K_A plane in order to avoid the phase structure present in the positive K_A plane.

Later it was noticed that essentially the same result can be obtained in the weak coupling region by finding an action which retains its form under the Migdal-Kadanoff recursion relation [5]. Such an action, stable under the averaging process of the renormalisation group transformation, is the generalisation of a periodic Gaussian to the group manifold, in analogy with the central limit

theorem of statistics [8]. For SU(3), the renormalised trajectory in the weak coupling region is then found to be [5],

$$K_6 = -0.20\ K_F\ ,\ \ K_A = -0.69\ K_F\ . \tag{5.1.5}$$

Symanzik's Perturbative Improvement Programme

The Migdal-Kadanoff renormalisation scheme does not produce the long range interactions which are generated by a block transformation. Therefore, though the above trajectories do a good job of circumnavigating the phase structure of the lattice gauge theories in the strong coupling region, they do not get rid of irrelevant lattice operators obscuring the continuum behaviour of the theory. This job can be accomplished by performing a perturbation expansion in the lattice spacing a, and then including suitable longer range interactions in the action to systematically get rid of the unwanted higher dimension terms [9].

Let us start with the simple plaquette action (cf. Eq.(2.1.6)). An expansion in the lattice spacing a gives,

$$\mathrm{Re}\,Tr\,(U_{plaq}) \ = \ -\frac{1}{4}a^4 F_{\mu\nu}F^{\mu\nu} + \frac{1}{12}a^6 D_\mu F_{\mu\nu} D_\mu F_{\mu\nu} + O(a^8)\ , \tag{5.1.6}$$

where D_μ is the covariant derivative. The first step in improving this classical action is to cancel off the $O(a^6)$ term. This can be accomplished in a variety of ways. Two of the possibilities are [10],

$$A[U] \ = \ \frac{2N}{g^2}\,\mathrm{Re}\,[\ \frac{5}{3}\sum Tr\,U_{plaq} - \frac{1}{12}\sum Tr\,U_{6p}\ ]\ , \tag{5.1.7a}$$

$$A[U] \ = \ \frac{2N}{g^2}\,\mathrm{Re}\,[\ \sum Tr\,U_{plaq} + \frac{1}{12}\sum Tr\,U_{8t}\ ]\ , \tag{5.1.7b}$$

where the sums are over all sites and all positive orientations of the loops. The various loops used here are shown in Fig. 5.5. This simple modification of the classical action results in the tree-level or leading log improvement of the full

quantum action [10]. As far as the ease of numerical simulation is concerned, the first choice is the more convenient one and so we will stick with it.

To improve the action at higher loop levels, one has to ensure that the continuum and lattice expressions for the expectation value of any Wilson loop match [11]. This is equivalent to saying that after the corrections for the difference in the lattice and continuum measures are made, the lattice propagator for the field,

$$f_{\mu\nu}(k) = i(\hat{k}_\mu A_\nu(k) - \hat{k}_\nu A_\mu(k)) , \qquad (5.1.8)$$

has no corrections to the $O(k^{-2})$ behaviour of the continuum propagator†. Here, $\hat{k}_\mu$ is the Fourier transform of the discrete derivative,

$$\hat{k}_\mu = \frac{2}{a}\sin(\frac{1}{2}k_\mu a) . \qquad (5.1.9)$$

The tree-level improvement in Eq.(5.1.7) gets rid of all the $ln(ka)$ dependence of the propagator [10]. One loop improvement corresponds to removing all $\sum_\mu k_\mu^4$ and $(k^2)^2$ terms from the propagator, and it can be achieved by including a non-planar 6-link operator with coefficient $O(g^2)$ [11]. The coefficients of the simple plaquette and 6-link rectangular operators also change by $O(g^2)$. For the numerically evaluated coefficients, one should look up Ref.[11].

Renormalisation Group Improvement

This is the approach followed by Wilson in his original paper [12]. The calculation proceeds similarly to the previous case. There the criterion for improving the action was the restoration of Lorentz invariance, which is ensured by removal of terms other than $O(k^{-2})$ from the propagator. However, here

† Remember that the inverse propagator for a scalar free particle on the lattice behaves like, $a^{-2}\sum_\mu \sin^2(k_\mu a) = k^2 + O(k^4 a^2)$.

the criterion changes to the functional form of the expectation value of the Wilson loop (or equivalently the propagator adjusted for the change in the integration measure) remaining invariant under the renormalisation group transformation.

Once a particular renormalisation group transformation is chosen,

$$U^1 = \int dU\, P(U^1, U)\,, \tag{5.1.10}$$

it can be converted into a relation $A^1(k) = R_b(A(k))$, using weak coupling expansion and Fourier transforms. Then the coefficients of the improved action can be fixed by the condition that the functional form of the propagator is the same on both the original and the blocked lattice. Obviously, the form of the improved action is dependent on the particular renormalisation group transformation used, but this is no surprise. For the SU(2) theory, Wilson determined, for the renormalisation group transformation he used (cf. section 3.3), the renormalisation group improved action to be [12],

$$A[U] = \frac{4}{g^2}[4.376\sum TrU_{plaq} - 0.252\sum TrU_{6p} - 0.17\sum TrU_{6t}]\,. \tag{5.1.11}$$

Similar calculation is in progress for the $\sqrt{3}$ blocking transformation used here.

There is one important drawback of these latter two approaches. Because of the fact that they are based on perturbative analysis, they completely miss the non-perturbative effects related to the non-trivial topology of the group. In the lattice theories, such effects typically manifest themselves as a phase structure in the extended action space involving higher dimensional representations of the group. For example, the SU(2) action in the adjoint representation describes the O(3) gauge theory, which is identical to the SU(2) theory as far as the perturbative behaviour is concerned. But we know that the behaviour of the two theories are drastically different from each other at long distances (one

obeys area law for large Wilson loops; the other doesn't), because of the difference in the topology characterised by the centre Z(2). This difference shows up as the non-trivial phase structure in the $[K_F,K_A]$ plane. Present Monte-Carlo calculations are being done in a region quite close to this phase structure, and therefore it is important to take into account the effects of such phase structures when finding an improved action. The Migdal-Kadanoff approach does succeed in finding the effect of the phase structures on the improved action, but it suffers from the lack of long distance interactions in the improved action. What we need is a combined approach which can take into consideration both the non-perturbative and the long range interactions. This is the subject of study for the rest of the chapter and as will be evident from the results; the Monte-Carlo renormalisation group analysis indeed achieves both the objectives.

5.2 : Improvement using Monte-Carlo Renormalisation Group

Under a renormalisation group transformation, all starting trajectories close to the RT converge toward it. Since the ideal improved action is just the basis vector defining the RT, to find the improved action, all one has to do is to determine the renormalised action generated in an MCRG calculation. Such an action typically involves an infinite number of couplings. From the standpoint of numerical efficiency, however, one needs to find an action that is both local (involves only small Wilson loops) and close to the RT. In this section, an iterative procedure for implementing this idea is described [13]. The numerical results presented in the next section will show that the method is quite successful, and also provides information on the distance of the starting action from the RT and the rate of convergence towards it.

The distance of the starting action from the RT is given by the magnitudes of the irrelevant lattice operators. As one performs renormalisation group transformations, the effect of these operators decreases. Therefore, the first block transformation is the one most sensitive to the effect of the irrelevant operators, and, to find the RT accurately, one should find the flow of the renormalised action at the first step in the blocking procedure. On the other hand, if the starting action is too far away from the RT, one block transformation will not take it sufficiently close to the RT, and several iterations will be needed to find a good approximation to the RT.

Consider an arbitrary line YZ (Fig. 3.5) in a two coupling constant space $[K_1,K_2]$ and assume that it lies inside the domain of attraction of the RT. Then, to find the RT, one would like to follow the evolution of the starting action $\{K^A\}$ under the renormalisation group transformation, i.e., determine the couplings at the points A^1, A^2, etc. In the MCRG calculation for the β-function, one does not determine the renormalised action. One just finds another point $\{K^B\}$ on the line YZ that is related to the point $\{K^A\}$ by a fixed scale transformation. This is achieved by matching the long distance behaviour of the two theories. In this process, expectation values of several (as many as we care to evaluate) operators for points $\{K^B\}$ and $\{K^{A^1}\}$ are calculated. Note that these have been measured on lattices which have the same size and boundary conditions. If the two actions are the same (i.e., same expectation values), then the line YZ would be a flow line and the first step in the iteration is complete. Otherwise, we want to find the action $\{K^{A^1}\}$ which is closer to the RT.

Assume that all the expectation values, Ω_i, are analytic functions of the couplings. Then to first order the expectation values calculated at $\{K^B\}$ can be expanded about those at $\{K^{A^1}\}$ as,

$$<\Omega_i>_B \;\sim\; <\Omega_i>_{A^1} + \frac{\partial<\Omega_i>}{\partial K_j}\,\Delta K_j \quad . \tag{5.2.1}$$

The rate of change, $\frac{\partial <\Omega_i>}{\partial K_j}$, is the connected correlation function $<:\Omega_i \Omega_j:>$. Thus we get,

$$<\Omega_i>_B \sim <\Omega_i>_{A^1} + <:\Omega_i \Omega_j:>_{A^1} \Delta K_j \ . \qquad (5.2.2)$$

From this equation we can calculate the difference in the couplings,

$$\Delta K_j \equiv K_j^B - K_j^{A^1} \ , \qquad (5.2.3)$$

by a simple matrix inversion. A consistency check is to expand $<\Omega_i>_{A^1}$ about $\{K_B\}$,

$$<\Omega_i>_{A^1} \sim <\Omega_i>_B - <:\Omega_i \Omega_j:>_B \Delta K_j \ . \qquad (5.2.4)$$

and compare the two $\{\Delta K_j\}$. Their closeness to each other can be used as a check to ensure the validity of the linear extrapolation, and the mean $\{\Delta K_j\}$ are correct to 2^{nd} order. To show the statistical accuracy and stability of the linear approximation, we use various starting points $\{K^B\}$ for the same $\{K^A\}$ and check whether they all yield the same $\{\Delta K_j\}$. This, in practice, does not involve additional computer time since in doing an MCRG calculation of the β-function a number of nearby points $\{K^B\}$ are already explored. We repeated this process for several points $\{K^A\}$ and determined the change in the various ratios K_i / K_F as a function of K_F. This provided information on the shape of the RT and also showed which couplings are important in a given region.

If after the first step the change $\{\Delta K_j\}$ is small, and the new couplings are,

$$K_j^1 \equiv K_j^B - \Delta K_j \ , \qquad (5.2.5)$$

then all the data at $\{K^B\}$ can be reweighed by the difference in the Boltzmann factor to get a distribution at $\{K^1\}$. This is possible if the data sample at $\{K^B\}$ is large enough so as to have enough data at configurations which have a large

probability of occurrence at $\{K^1\}$. If the reweighing gives a statistically significant sample, then one can go back to Eq. (5.2.2) and calculate the new change in the couplings and proceed iteratively until the method converges or the extrapolation fails.

In case the method fails at step n (which can include the first), a fresh set of expectation values is generated by a new MC simulation with the best guess for the new couplings at that stage. If this indeed is an improved action, then the new $\{\Delta K_j\}$ would be smaller. The power of this method is in its recursive nature, and using it iteratively the RT can be found very accurately for any RG transformation and for any value of the coupling.

A slightly different method has been used by Swendsen [14] to find the improved Hamiltonian for the 2-dim Ising model. He used the expectation values at points $\{K^A\}$ and $\{K^{A^1}\}$ to find $\{\Delta K_j\}$. These points have the same physical size and boundary conditions. Moreover, since the statistical data at these two points are correlated, the errors are smaller. In his analysis, the new couplings were found essentially by reweighing the data by the difference in the Boltzmann factor till the expectation values matched. For the 2-dim, Ising model there is no problem with the statistical strength of the data, since one can simulate the system at the critical point directly. But in other cases, as mentioned earlier, the results are not reliable when the $\{\Delta K_j\}$ are large. The reliability of the results can be checked by calculating the connected correlation functions and verifying how well the consistency condition (Eqs.(5.2.2) and (5.2.4)) is satisfied. The method described in this section proves to be better for two reasons :

(i) The points $\{K^B\}$ can be chosen such that the $\{\Delta K_j\}$ are small.

(ii) The accuracy of the $\{\Delta K_j\}$ can be explicitly verified by checking how well the different $\{K^B\}$ points produce the same answer.

5.3 : Results for SU(2)

We did not estimate the error in $\{\Delta K_j\}$ for each point $\{K^B\}$ at fixed $\{K^A\}$. Instead, after using the consistency check, Eqs. (5.2.2) and (5.2.4), to define the useful set of points $\{K^B\}$, the statistical error was estimated by simply treating each of those points as independent. A more careful analysis would require one to assign relative weights to the different points $\{K^B\}$ based on their statistical weight and the change $\{\Delta K_j\}$. At this stage, the systematic errors from the number of operators kept are far more severe. The validity of the results will therefore have to be tested by repeating the calculation using the improved action determined here.

The action in the $[K_F, K_A, K_{3/2}, K_{6p}, K_{6l}, K_{6t}]$ space is defined in Eq. (3.1.1). We used 7 starting points $\{K^A\}$ along the M-K line and 5 along the Wilson axis. The number of points $\{K^B\}$ that satisfied the consistency condition for each $\{K^A\}$, ranged from 7 to 15 as listed in the tables.

In deciding what operators to keep we noticed a decoupling between the higher spin representations and the 6-link loops. For example, the addition of $K_{3/2}$ largely affected K_F and K_A, and the addition of K_{6t} mostly affected K_F and K_{6p}. Both the statistics (due to critical slowing down) and the distance from the RT become worse as g_{bare} is decreased. Because of this the total number of operators that could be determined accurately also decreased as K_F increased. This is at present a limitation since the renormalised couplings depend on the number of operators used. However, within each set of couplings included we found a definite pattern, and by considering various $\{K^A\}$ we are

able to make statements about the RT.

In Table 5.1, the effect of keeping various combinations of operators is shown for K_F=3.7 on the M-K line. Next, the improved action in the the $[K_F, K_A, K_{6p}]$ space is displayed in Table 5.2 as a function of K_F. We show the effects of adding $K_{3/2}$ and K_{6t} to this set in Tables 5.3 and 5.4, respectively. This makes up the largest set of operators that we could use in the improved action analysis with the present data.

In the central range of the couplings explored by us, the flows from both the Wilson axis and the M-K line, when projected in the $\{K_F, K_A\}$ plane, converge to an approximate trajectory given by $K_A \sim -0.16\, K_F$. The Grossman-Samuel β-function (cf. Eqs.(4.1.6-4.1.7)) is almost flat along this line; i.e., there are no corrections to the 1-loop asymptotic value. This is indeed the behaviour expected from the RT, a fast and smooth approach to the fixed point.

The trajectory shifts by a significant amount upon the addition of $K_{3/2}$. K_A takes on a larger negative value while $K_{3/2}$ provides a compensating positive term. The projection of the improved action is now very close to the result found using the M-K approximation [6]. This suggests that the corresponding RT's lie close together in this region. Our results show that in this region $K_{3/2}$ contribution cannot be neglected even though it is small (~5%), and we conclude that it is necessary to include higher representations in the improved action.

The results showed a dramatic improvement when the 6-link planar loop coupling K_{6p} was added. In the $[K_F, K_A, K_{3/2}, K_{6p}]$ space, the spread of points obtained with different $\{K^B\}$ became small and the $\{\Delta K_i\}$ obtained from Eqs. (5.2.2) and (5.2.4) converged. As g_{bare} was made smaller, the ratio K_{6p}/K_F increased and seemed to be approaching the tree-level improved value -0.05 [10,11], while the effect of the higher representations decreased. The other two 6-link couplings K_{6t} and K_{6l} had positive coefficients with K_{6t} being more

stable. As shown in Table 5.4, the inclusion of K_{6t} made the coupling K_{6p} much more negative and the strength of K_{6t} decreased with increasing K_F.

An advantage of this method is that both the perturbative (6-link couplings) and non-perturbative (higher representation couplings) effects can be analysed simultaneously. The fact that the Wilson and M-K actions lie on opposite sides of the RT for the coupling K_A and yet both of them converge to approximately the same trajectory after the first iteration, implies that the points $\{K^{A^1}\}$ are close to the RT, in the limited coupling space we have explored. We are therefore able to map an approximate RT over a large range of couplings and the results in Tables 5.2, 5.3 and 5.4 show that it is not linear just beyond the crossover region.

We found that, for a given starting $\{K^A\}$, the renormalised coupling $K_F^{A^1}$ was much smaller than the value of K_F^B for which the long distance behaviour of the theory differs from K_F^A by the scale factor of the RG transformation. To see this, compare the difference between K_F^A and K_F^1 in Tables 5.1, 5.2, 5.3 and 5.4 and the value of ΔK_F found in the MCRG calculation. This feature is consistent with the observation that, if we try to match the variables on the $(3\sqrt{3})^4$ lattices, the ΔK_F so obtained would be large. Such a large discrepancy implies that the starting points $\{K^A\}$ are far from the RT.

The calculation of the improved action is very sensitive to the number of operators included. To improve the statistics and to check the stability of the improved action obtained here, we are currently running the programme on an 18^4 lattice.

5.4 : Results for SU(3)

The results in the $[K_F, K_{6p}, K_{6l}, K_{6t}, K_6, K_A]$ space are shown in Table 5.5. We were able to use only four $(3\sqrt{3})^4$ lattices for both K_F^A=6.5 and 7.0. These are much fewer K_B points than those used in the SU(2) case; however, the consistency condition worked well and the coefficients of all the 6 operators could be determined in the improved action. The small magnitudes of all the new couplings in K^{A^1} supports our previous claim that the simple plaquette action is quite close to the RT.

The higher dimensional representations and the 6-link operators were again found to be decoupled. The 6-link operators had the same signs that they had for SU(2), and the higher representation operators had the same signs as predicted in Ref.[5] (cf. Eq.(5.1.5)). The small contribution of the higher representation operators means that the effect of the non-trivial phase structure is smaller here than in the SU(2) case. This is a surprising result, since for SU(3) the phase structure in the $[K_F\ ,\ K_A]$ plane is known to lie closer to the Wilson axis than for SU(2) [15].

5.5 : Conclusions

We briefly enumerate the main results and lessons of this whole analysis :

1) An MCRG calculation does not require much more time than any other reliable Monte-Carlo calculation. Dedicated super computers or special purpose computers are required for both.

2) The $\sqrt{3}$ transformation is very efficient for the 4-dim gauge theories. Its peculiar geometry is not a drawback.

3) Both for SU(2) and SU(3), the non-perturbative β-function differs from the 2-loop result at the $\sim$10% level, because of the phase structure in the extended coupling constant space. This is true well beyond the crossover region. Therefore, to check the scaling of long distance observables, one should use the results of an MCRG calculation.

4) A good estimate for the renormalised trajectory can be found using the iterative method proposed. The RT for SU(2) interpolates between the results of Migdal-Kadanoff approximate renormalisation and Symanzik's perturbative improvement programme. The results for SU(3) show that, starting with the Wilson action, the RT is reached after just one block transformation.

5) An improved action approach is a must to see scaling and to approach the continuum limit faster.

Lastly we outline how MCRG can be used to calculate the long distance properties of QCD. The discussion will be restricted to the pure gauge theory; fermions can be put in as external sources to obtain the results in the valence approximation in the standard way.

An improved action obtained from an MCRG calculation is used to update an $(N\sqrt{3})^4$ lattice. The lattice size $N\sqrt{3}$ is selected after taking into account all finite size effects; i.e., the largest correlation length should be a factor of $\sim$3 smaller than it. On the basis of the auto-correlation length and the measurement to update time, configurations separated by a certain number of update sweeps are blocked down to N^4 lattices. The important point here is that the theory on the N^4 lattice has the same long distance behaviour as the original theory, but the irrelevant short distance operators are suppressed. The ratio of the lattice correlation length to the lattice size remains unchanged since both are reduced by the same $\sqrt{3}$ scale factor. The block variables are now used for

constructing appropriate interpolating field operators and calculating their long distance correlations.

The completion of the MCRG procedure yields both the β-function needed to check scaling and an improved estimate of the renormalised trajectory. This last step, which includes generating configurations on an N^4 lattice for comparing the block variables, is ~30-50% overhead on the $(N\sqrt{3})^4$ update time. This calculation is currently in progress.

REFERENCES

[1] M. Luscher and P. Weisz, in preparation.

[2] M. Luscher and P. Weisz, DESY preprint, DESY 84-018 (1984).

[3] A. A. Migdal, Zh. Eksp. Teor. Fiz. 69 (1975) 810.

A. A. Migdal, Zh. Eksp. Teor. Fiz. 69 (1975) 1457.

[4] L. P. Kadanoff, Ann. Phys. 100 (1976) 359.

[5] D. Horn and C. K. Zachos, Phys. Rev. D29 (1984) 1202.

[6] K. M. Bitar, S. Gottlieb and C. K. Zachos, Phys. Rev. D26 (1982) 2853.

[7] G. Bhanot and M. Creutz, Phys. Rev. D24 (1981) 3213.

[8] G. Jona-Lasinio, Nuov. Cim. 26B (1975) 99.

[9] K. Symanzik, in *Mathematical Problems in Theoretical Physics*, ed. R. Schrader et al, Springer, Lecture Notes in Physics 153 (1982).

[10] G. Curci, P. Menotti and G. Paffuti, Phys. Lett. 130B (1983) 205.

S. Belforte, G. Curci, P. Menotti and G. Paffuti, Phys. Lett. 136B (1983) 399.

[11] P. Weisz, Nucl. Phys. B212 (1982) 1.

P. Weisz and R. Wohlert, DESY preprint, DESY 83-091.

[12] K. Wilson, in *Recent Developments in Gauge Theories* (Cargese 1979), ed. by G. 'tHooft et al, Plenum Press, New York (1980).

[13] R. Gupta and A. Patel , CALT-68-1121 (1984).

R. H. Swendsen, *Real Space Renormalisation* in *Topics in Physics, Vol. 30*, Springer Verlag (1983).

[14] R. H. Swendsen, Phys. Rev. Lett. 52 (1984) 1165.

[15] G. Bhanot, Phys. Lett. 108B (1982) 337.

FIGURE CAPTIONS AND FIGURES

[5.1]Migdal's approximate renormalisation procedure.

[5.2]Kadanoff's approximate renormalisation procedure in which the transverse interactions such as D are moved away, before integrating out the interactions such as A, B and C by summing over the degrees of freedom denoted by crosses.

[5.3]Kadanoff's approximate renormalisation procedure in which the longitudinal interactions are moved using Fourier transform.

[5.4]The projection of the trajectories for the Migdal-Kadanoff approximate renormalisation scheme onto the $[K_F, K_A]$ space for the SU(2) gauge theory.

[5.5]Various Wilson loops used in Symanzik's perturbative action improvement programme.

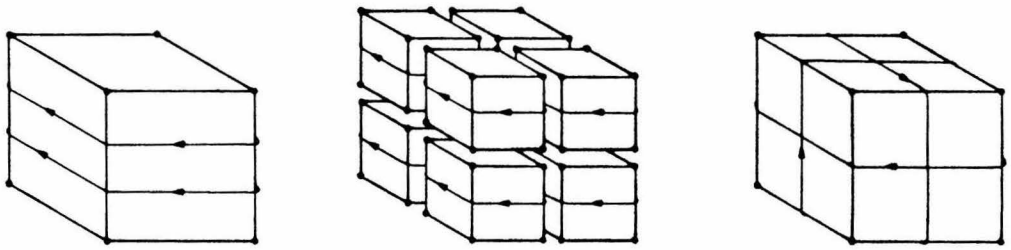

Fig. 5.1

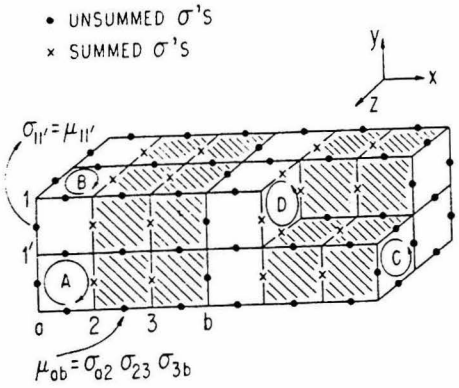
• UNSUMMED σ'S
× SUMMED σ'S
y
x
z
$\sigma_{11'} = \mu_{11'}$
1
1'
B
D
A
C
a
2
3
b
$\mu_{ab} = \sigma_{a2}\,\sigma_{23}\,\sigma_{3b}$

Fig. 5.2

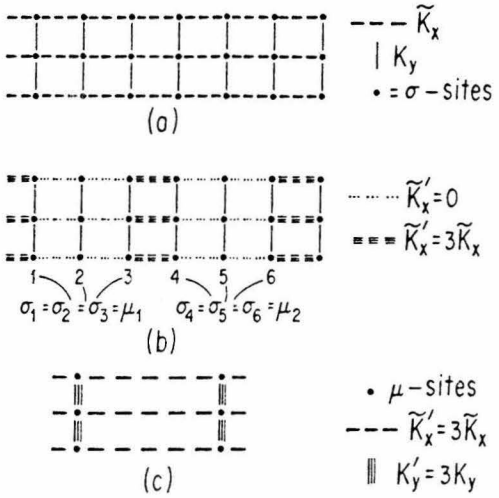
$\widetilde{K}_x$
K_y
• = σ – sites
(a)
$\widetilde{K}'_x = 0$
$\widetilde{K}'_x = 3\widetilde{K}_x$
1 2 3 4 5 6
$\sigma_1 = \sigma_2 = \sigma_3 = \mu_1$
$\sigma_4 = \sigma_5 = \sigma_6 = \mu_2$
(b)
• μ – sites
$\widetilde{K}'_x = 3\widetilde{K}_x$
$K'_y = 3K_y$
(c)

Fig. 5.3

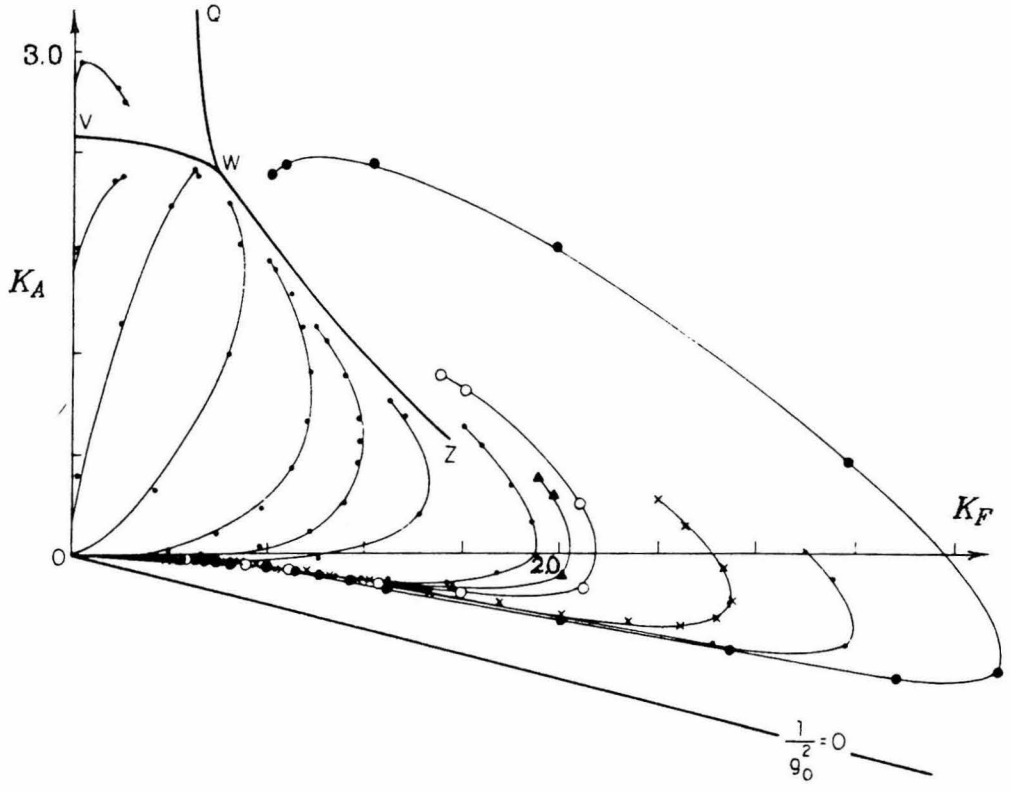
3.0
Q
V
W
K_A
Z
K_F
0
20
$\frac{1}{g_0^2} = 0$

Fig. 5.4

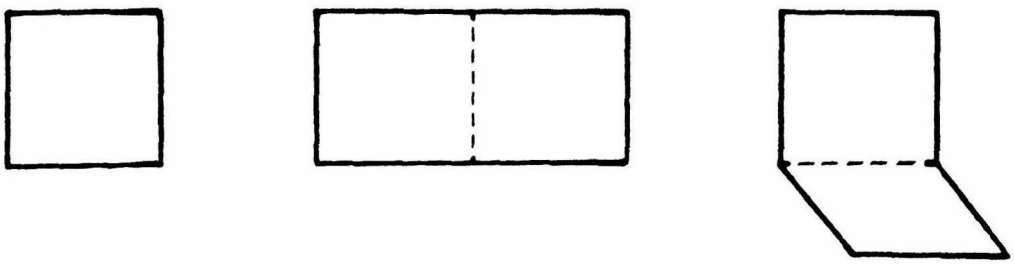

plaq 6p 6l

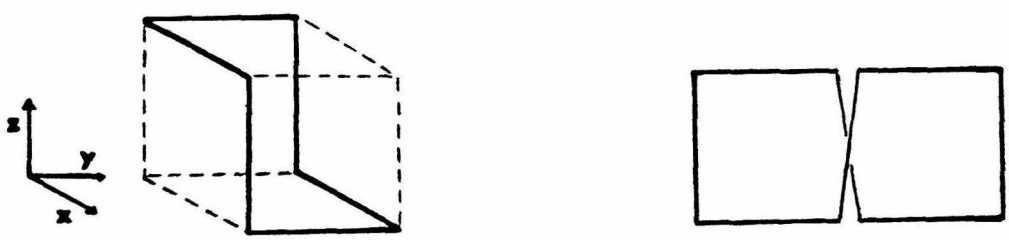

6t 8t

Fig. 5.5

TABLES

No. of $\{K^B\}$ pts. used	Improved action couplings					
	K_F	K_A / K_F	$K_{3/2} / K_F$	K_{6p} / K_F	K_{6l} / K_F	K_{6t} / K_F
12	2.614(7)	-.167(1)				
12	2.741(7)	-.233(1)	.056(1)			
11	2.783(6)	-.229(2)	.055(1)	-.0056(6)		
11	2.048(8)	-.236(3)	.054(3)	-.080(1)		.142(2)
2	2.193(1)			-.006(1)		
11	2.660(4)	-.165(1)		-.0061(6)		
2	1.58(2)			-.106(1)		.182(4)
8	1.968(5)	-.177(2)		-.082(2)		.150(2)
2	1.032(4)			-.182(2)	.109(4)	.136(7)
6	1.42(2)	-.207(3)		-.131(1)	.071(2)	.106(3)
6	1.51(1)	-.287(8)	.069(7)	-.123(1)	.067(1)	.100(2)

Table 5.1 : Various projections of the renormalised SU(2) action for the starting action K_F=3.7 along the M-K line. The errors in parentheses are calculated assuming each $\{K^B\}$ point to be independent.

Projection of the improved action in the $[K_F, K_A, K_{6p}]$ space				
Starting action $\{K^A\}$	No. of $\{K^B\}$ pts. used	K_F	K_A / K_F	K_{6p} / K_F
3.7 $(M-K)$	11	2.660(4)	-.165(1)	-.0061(06)
4.0 $(M-K)$	12	2.923(5)	-.154(3)	-.0186(16)
4.35$(M-K)$	12	3.225(7)	-.144(1)	-.0283(07)
4.7 $(M-K)$	15	3.504(6)	-.135(1)	-.0323(03)
5.05$(M-K)$	12	3.807(5)	-.131(1)	-.0367(02)
5.2 $(M-K)$	13	3.915(6)	-.129(1)	-.0370(03)
5.5 $(M-K)$	9	4.181(7)	-.130(1)	-.0381(03)
2.5 (W)	10	2.491(5)	-.145(1)	-.0041(06)
2.75 (W)	15	3.007(6)	-.140(2)	-.0216(15)
3.0 (W)	15	3.476(9)	-.124(1)	-.0335(06)
3.25 (W)	15	3.936(7)	-.114(1)	-.0392(02)
3.5 (W)	13	4.43(1)	-.112(1)	-.0427(02)

Table 5.2 : Projection of the renormalised SU(2) action for different starting actions. The errors in parentheses were calculated assuming each $\{K^B\}$ point to be independent.

Projection of the improved action in the $[K_F, K_A, K_{3/2}, K_{6p}]$ space					
Starting action $\{K^A\}$	No. of $\{K^B\}$ pts. used	K_F	K_A / K_F	$K_{3/2} / K_F$	K_{6p} / K_F
3.7 $(M-K)$	11	2.783(6)	-.229(2)	.055(1)	-.0056(06)
4.0 $(M-K)$	12	3.091(7)	-.221(3)	.050(1)	-.0178(15)
4.35$(M-K)$	12	3.42(1)	-.211(2)	.044(1)	-.0268(11)
4.7 $(M-K)$	14	3.73(1)	-.202(3)	.041(2)	-.0305(04)
5.05$(M-K)$	12	4.07(2)	-.196(3)	.037(2)	-.0345(03)
5.2 $(M-K)$	11	4.18(2)	-.193(3)	.036(2)	-.0348(03)
5.5 $(M-K)$	9	4.44(3)	-.186(7)	.029(3)	-.0359(05)
2.5 (W)	8	2.571(5)	-.195(1)	.043(1)	-.0036(03)
2.75 (W)	14	3.16(1)	-.199(3)	.042(2)	-.0208(15)
3.0 (W)	12	3.69(1)	-.190(4)	.040(2)	-.0314(07)
3.25 (W)	14	4.12(2)	-.160(5)	.025(3)	-.0374(04)
3.5 (W)	13	4.71(2)	-.168(5)	.028(3)	-.0402(04)

Table 5.3 : Projection of the renormalised SU(2) action for different starting actions. The errors in parentheses were calculated assuming each $\{K^B\}$ point to be independent.

Projection of the improved action in the $[K_F, K_A, K_{6p}, K_{6t}]$ space					
Starting action $\{K^A\}$	No. of $\{K^B\}$ pts. used	K_F	K_A / K_F	K_{6p} / K_F	K_{6t} / K_F
3.7 $(M-K)$	8	1.968(5)	-.177(2)	-.082(2)	.150(02)
4.0 $(M-K)$	11	2.19(1)	-.153(3)	-.090(1)	.130(2)
4.35$(M-K)$	12	2.46(1)	-.145(2)	-.093(1)	.117(1)
4.7 $(M-K)$	13	2.68(1)	-.135(2)	-.097(1)	.118(1)
5.05$(M-K)$	11	2.93(1)	-.131(1)	-.095(1)	.106(1)
5.2 $(M-K)$	11	3.03(2)	-.129(1)	-.097(1)	.107(1)
5.5 $(M-K)$	9	3.21(1)	-.134(2)	-.095(1)	.104(1)
2.5 (W)	7	1.774(8)	-.139(2)	-.081(2)	.157(2)
2.75 (W)	14	2.195(9)	-.131(2)	-.096(1)	.138(2)
3.0 (W)	14	2.55(1)	-.109(2)	-.102(1)	.126(1)
3.25 (W)	13	2.91(1)	-.106(2)	-.104(1)	.119(1)
3.5 (W)	14	3.35(1)	-.107(2)	-.100(1)	.106(1)

Table 5.4 : Projection of the renormalised SU(2) action for different starting actions. The errors in parentheses were calculated assuming each $\{K^B\}$ point to be independent.

Projection of the improved action for SU(3) in the $[K_F, K_{6p}, K_{6l}, K_{6t}, K_6, K_A]$ space

Coupling	K_F=6.5		K_F=7.0	
K_F	5.99(07)	5.53(04)	6.47(16)	5.96(19)
K_{6p} / K_F	-.033(1)	-.038(1)	-.035(2)	-.040(2)
K_{6l} / K_F		.015(3)		.014(2)
K_{6t} / K_F	.041(1)	.025(4)	.041(1)	.027(2)
K_6 / K_F		-.014(7)		-.003(1)
K_A / K_F	-.030(4)	-.019(4)	-.028(1)	-.024(1)

Table 5.5 : Projection of the renormalised SU(3) action for different starting actions along the Wilson axis. The errors in parentheses were calculated assuming each $\{K^B\}$ point to be independent.